Plant Biotechnology Journal
Open Access

Plant Biotechnology Journal (2025) **23**, pp. 3879–3899 doi: 10.1111/pbi.70182

OsDUF2488 acts synergistically with OsPrx1.1, regulates ROS metabolism and promotes dehydration tolerance in rice

Dipak Gayen[1,a], Sunil Kumar[1,†], Pragya Barua[1,†], Nilesh Vikram Lande[1,†,b], Subhasis Karmakar[2], Amit K. Dey[3], Saurabh Gayali[1], Tushar Kanti Maiti[3], Kutubuddin Ali Molla[2], Snehal Murumkar[1], Subhra Chakraborty[1] and Niranjan Chakraborty[1,*]

[1]*BRIC-National Institute of Plant Genome Research, Jawaharlal Nehru University Campus, New Delhi, India*
[2]*ICAR-National Rice Research Institute, Cuttack, India*
[3]*Regional Centre for Biotechnology, NCR Biotech Science Cluster, Faridabad, Haryana, India*

Received 14 November 2024;
revised 21 May 2025;
accepted 23 May 2025.
**Correspondence* (Tel 91-11-26735178; fax 91-11-26742658; email nchakraborty@nipgr.ac.in)
[a]Present address: Department of Biochemistry, Central University of Rajasthan, Ajmer, India
[b]Present address: Punyashlok Ahilyadevi Holkar College of Agriculture, Ahmednagar, Maharashtra, India
[†]These authors contributed equally to this work.

Keywords: antioxidant defence, dehydration tolerance, energy-converting organelles, proteome map, redox homeostasis, stress adaptation.

Summary

Stress-mediated regulation of energy metabolism and its relation to plant adaptation remain largely unknown. Mitochondrial redox potential is greatly influenced by stress-induced reactive oxygen species (ROS); therefore, we mapped the dehydration-induced alterations in the mitochondrial proteome of a resilient rice cultivar, Rasi, generating a proteome map representing the largest inventory of dehydration-responsive mitochondrial proteins from any plant species. Quantitative proteomic analysis led to the identification of an array of dehydration-responsive proteins (DRPs), associated with various cellular functions, conceivably impinging on the molecular mechanism of adaptation. One DRP identified in the mitochondrial proteome was yeast cadmium factor 54 (YCF54-like), also known as DUF (domain of unknown function) and hereafter referred to as OsDUF2488. We demonstrated that OsDUF2488 localises to mitochondria and preferentially interacts with peroxiredoxin, OsPrx1.1. Overexpression of OsDUF2488 in rice caused enhanced tolerance to dehydration and oxidative stress, while CRISPR/Cas9 knockout mutants of OsDUF2488 showed hypersensitivity to dehydration. Upon exposure to dehydration, OsDUF2488 could rescue mitochondrial dysfunction, contributing to increased ATP production in OsDUF2488-overexpressing rice. Coexpression of OsDUF2488 and OsPrx1.1 in yeast demonstrated a mutual effect on enhanced ROS catabolism, suggesting a cross-kingdom adaptive response of OsDUF2488. Our findings suggest that OsDUF2488 acts synergistically with OsPrx1.1 to regulate redox homeostasis and promote stress tolerance in rice.

Introduction

Water-deficit stress or dehydration limits plant growth and development, affecting crop productivity more than any other environmental risk factors do. One of the components that decides the impact of dehydration on crop productivity, besides photosynthesis, is its effect on mitochondrial respiration (Atkin and Macherel, 2008). Mitochondria, one of the most important organelles, contribute to the production of metabolic energy through oxidative phosphorylation, and are universally distributed across species in the three cellular domains (Jacoby *et al*., 2012). Reactive oxygen species (ROS) are an important consequence of aerobic metabolism produced in organelles with a sustained electron flow, especially chloroplasts (Dietz and Pfannschmidt, 2011), mitochondria (Huang *et al*., 2016) and peroxisomes (Sandalio and Romero-Puertas, 2015). Nevertheless, stress-induced enhanced production of ROS is primarily mitigated by redox homeostasis through coordinated stress responses in these organelles. It is well known that mitochondria act both as a source and target of cellular ROS, particularly more during stress-induced inhibition of the respiratory chain (Jacoby *et al*., 2012). In particular, mitochondrial ROS participate in respiratory function as well as phytohormone action and are incorporated into signalling pathways including those regulating cell defence and stress responses (Dunn *et al*., 2015; Huang *et al*., 2016). Hence, mitochondrial malfunction causes excessive production of ROS and altered responses to abscisic acid and calcium signalling and represses stress-responsive gene expression (He *et al*., 2012). While many facets of the metabolic cross-talk between mitochondria and chloroplasts, and their interdependence in maintaining redox status are known, the mechanism of how they are regulated is still largely unknown.

Rice, unlike other cereals, thrives on inundated soil, with over 50% of global rice-producing regions being rainfed and is thus hypersensitive to dehydration stress. It has the lowest water-use efficiency of all cereal crops. Owing to highly conductive cuticles, the water permeability of rice is high (Blum, 2009), resulting in high rates of transpiration and making irrigation a prerequisite throughout its life cycle. The consequence of water-deficit conditions, especially during key stages in the growth cycle, constrains the production of rice, with severe economic implications. Screening of dehydration response in rice, the world's most important food crop, is thus imperative to achieve insights into its resiliency.

In general, stress adaptation in plants involves reprogramming of cellular metabolism by diverting energy from developmental

processes to stress acclimatization. Specifically, the mitochondrial metabolic pathway is activated by intracellular signals generated when cells are stressed and regulated by stress-associated proteins. Dehydration-elicited oxidative stress is an imbalance between the production of ROS and the antioxidant defence systems. Since the involvement of mitochondria is central to ROS homeostasis under dehydration, the identification of potential protein markers remains an important but challenging target. Over the last two decades, mitochondrial stress response has been extensively studied in plants that include oxidative stress (Sweetlove *et al.*, 2002), anoxic stress (Millar *et al.*, 2004), hypersalinity (Chen *et al.*, 2009), cold (Tan *et al.*, 2012), flooding (Komatsu *et al.*, 2011; Mustafa and Komatsu, 2016), heat (Rurek *et al.*, 2018) and dehydration (Gayen *et al.*, 2019; Taylor *et al.*, 2005).

In this study, we started by looking at the physiological reactions to dehydration, such as changes in metabolism and adjustments to protein markers related to mitochondrial dynamics. We specifically focused on how plant cells respond to dehydration by stimulating their mitochondria and antioxidant defence system. Functional screening of the mitochondrial proteome of rice led to the identification of a yeast cadmium factor 54 (YCF54) (yeast cadmium factor), also known as DUF (domain of unknown function) protein, designated OsDUF2488, among an array of differentially regulated proteins. Interestingly, YCF54-like proteins have previously been reported to play a critical role in the synthesis or maturation of the cyclase subunit (Albus *et al.*, 2012; Hollingshead *et al.*, 2016). Our study demonstrated that OsDUF2488 predominantly expresses under dehydration and oxidative stress, and regulates the expression of a redox protein, OsPrx1.1. The experimental evidence suggests that OsDUF2488 localises predominantly to mitochondria and sparsely to chloroplasts. The coexpression of OsDUF2488 and OsPrx1.1 in yeast showed a synergistic effect on ROS homeostasis. More importantly, significantly, overexpression of OsDUF2488 in dehydration-sensitive IR64 background could maintain an appropriate redox homeostasis and promote stress resiliency, while the CRISPR/Cas9 knockout mutants showed hypersensitivity to dehydration.

Results

Growth responses to increasing dehydration, physicochemical characteristics and mitochondrial ultrastructure

To determine at what stage rice seedlings sense dehydration stress, the magnitude of their responses was monitored by multiple morpho-physicochemical indices. Relatively little phenotypic change such as leaf wilting was observed until 3 days of dehydration; the leaves rolled at 6 days, which aggravated further at 9 days, and the seedlings exhibited pronounced wilting (Figure 1a–d). Significantly, the alterations of physicochemical traits coincided with mitochondrial damage as observed by transmission scanning electron microscopy. The ultrastructure of mitochondria in dehydrated cells displayed alterations of cristae architecture, which were more noticeable under severe dehydration (Figure 1a–d). The soil moisture content (SMC), under unstressed conditions, was maintained at around 44%, which declined to 9% at 9 days of dehydration (Figure 1e). Consequently, leaf relative water content (RWC) was reduced from 90% to 65% (Figure 1f), while there was a 3-fold increase in proline abundance (Figure 1g). More importantly, H_2O_2 and malondialdehyde (MDA) contents were progressively increased with the severity of dehydration (Figure 1h,i). The net photosynthetic rate also declined by approximately 50% at 3 days (Figure 1j), with SMC still above 30%. The stomatal conductance declined linearly (Figure 1k) with a concomitant increase in intercellular CO_2 (Figure 1l) during 3–9 days of dehydration. Together, these results suggest that the rice seedlings could sense dehydration stress 3 days after exposure and respond in a stage-specific manner. Based on these observations, we selected mild (3-day), moderate (6-day) and severe (9-day) dehydration time points for downstream proteomic analysis.

Enrichment and integrity of mitochondria and purity of mitochondrial proteins

The mitochondria-enriched fraction was achieved by Percoll density gradient centrifugation (Gayen *et al.*, 2019). The fluorescent images of the Rhodamine-123-stained mitochondria were perfectly superimposable over the phase-contrast images, indicating the integrity and absence of other cytoplasmic organelles (Figure 2a). Next, the integrity of mitochondria was also examined by the activity of cytochrome c oxidase, which was remarkably increased by the addition of non-ionic detergent Triton X-100 (Figure 2b). The enrichment of mitochondrial proteins and cross-contamination of chloroplasts were sequentially monitored by immunoblot analysis using anti-COX II, anti-RuBisCo and anti-Lhcb1 antibodies. While there was a significant enrichment of the mitochondrial marker COX II compared to the cell lysate, the presence of RuBisCo was negligible. More significantly, no Lhcb1 could be detected in the mitochondria-enriched fraction (Figure 2c). These results indicate that the mitochondria-enriched fraction was devoid of chloroplastic contamination and the integrity of the membranes remains intact.

Dehydration-responsive mitochondrial proteome landscape

Dehydration-induced temporal changes in the mitochondrial proteome were examined by iTRAQ labelling, followed by LC–MS/MS analysis (Figure S1). The peptides subjected to LC–MS/MS analysis were identified at 1% global FDR. The proteomic analysis led to the identification of 589 proteins. Among the identified proteins, those having unused score ≥1.3 with at least two peptides were considered for relative protein expression. A total of 128 proteins were recognised by three replicates (Table S1). Furthermore, we considered only those proteins whose variance across the replicates varied <50%. A threshold of 1.5-fold was set to define changes in protein abundance, which led to the identification of 101 DRPs (Table S2). Only those proteins whose variance across the replicates varied <50%. The mitochondrial protein distribution and cumulative frequency are shown in relation to the percentage differences between the replicates (Figure S2a). Since mitochondrial proteins are distributed in the outer membrane, inner membrane and matrix, their physicochemical properties are expected to be greatly varied. The proteins were found to be almost evenly distributed throughout the pI range (pI 5–11) (Figure S2b). The molecular weights ranged from 20 to 150 kDa (Figure S2c). The proteins showed GRAVY values ranging from 0.6 to -1.2, suggesting a progressive variation in their hydrophobicity (Figure S2d). The mass spectrometry data have been submitted with the dataset identifier PXD022269 to the ProteomeXchange consortium through the

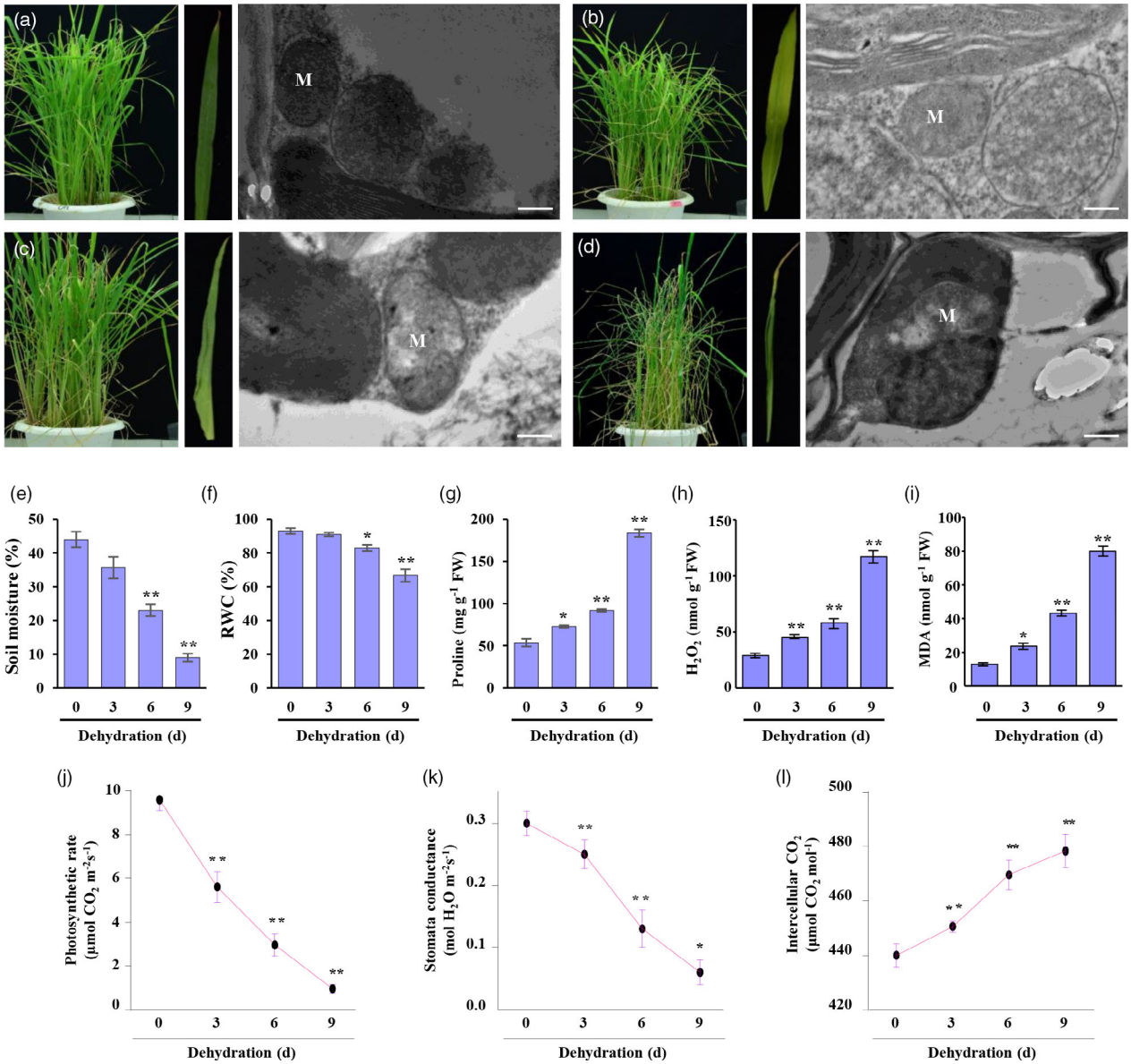

Figure 1 Morpho-physiological responses of 4-week-old rice seedlings exposed to dehydration over a period of 9 days, and changes in mitochondrial ultrastructure. (a–d) Dehydration-induced morphological changes of seedlings for 0-, 3-, 6-, and 9-day, respectively, along with a magnified view of the leaves and ultrastructural changes in mitochondria. M indicates mitochondria. Scale bar, 100 nm. (e–i) Effects of dehydration on SMC, RWC and proline content, and stimulated production of H_2O_2 and MDA, the secondary products of lipid peroxidation. The data were treated statistically and expressed as means ± SE of three independent experiments. The statistical significance of changes from that of unstressed seedlings is indicated by an asterisk (*P, 0.05; **P, 0.01). One-way ANOVA with DMRT post hoc test. (j–l) Effects of dehydration on net photosynthetic rate, stomatal conductance, and intercellular CO_2 are also shown. Data shown are the means ± SE of three independent experiments. The statistical significance of changes from that of unstressed seedlings is indicated by an asterisk (*P, 0.05; **P, 0.01). One-way ANOVA with DMRT post hoc test. MDA, malondialdehyde; RWC, relative water content; SMC, soil moisture content.

PRIDE partner repository. To gain a comprehensive overview of the protein expression profiles, hierarchical clustering was performed. The data were considered in terms of fold value change with respect to those of unstressed control, and the ratios were averaged across three replicates. The ratio was averaged across three replicates. The average fold values were log-transformed to the base 2 for heat map analysis (Figure 2d). Interestingly, among 73 high-abundance DRPs, 6 were shared by all dehydration stages, 30 DRPs shared by two stages (1 at 3-day and 6-day, 27 at 6-day and 9-day, and 2 at 9-day and 3-day), while 22, 6 and 9 DRPs specifically displayed increased abundance at 3-day, 6-day and 9-day, respectively (Figure 2e). A total of 71 DRPs were downregulated at least in one time point (Figure 2f), 2 DRPs in all time points, 33 in two time points (1 at 3-day and 6-day, 29 at 6-day and 9-day and 3 at 9-day and 3-day), while 24, 5 and 7 DRPs at 3-day, 6-day and 9-day, respectively. The intracellular localization of the DRPs was examined by multiple predicting programs such as TargetP, MitoFates, MitoProt, and

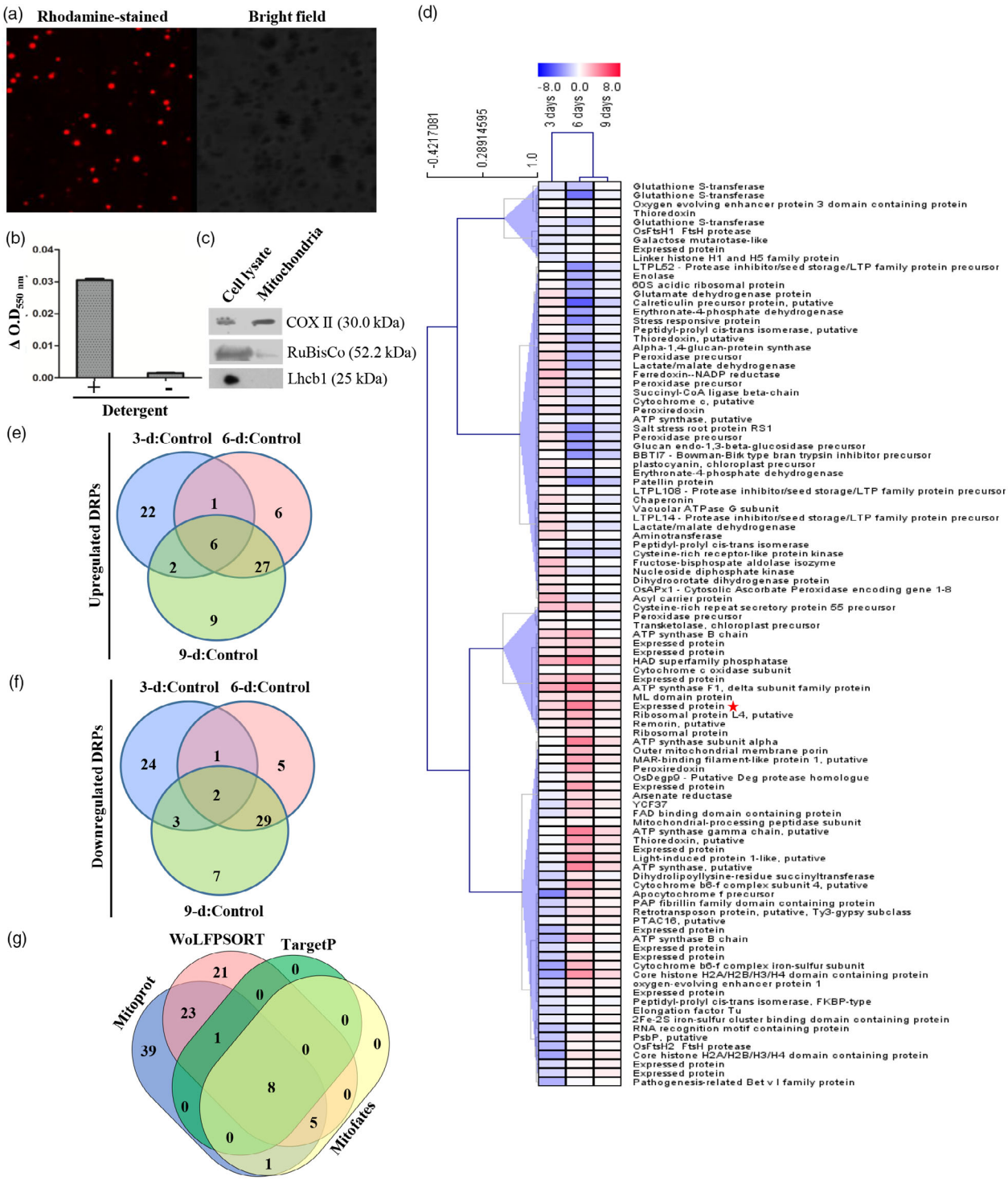

Figure 2 Mitochondrial integrity and fraction purity, and dehydration-responsive proteome dynamics. (a) Fluorescence image of Rhodamine-123-stained mitochondria and corresponding bright field image. Scale bar, 10 μm. (b) Cytochrome c oxidase activity in the presence (+) and absence (−) of non-ionic detergent Triton X-100. Data shown are the means ± SE of three independent experiments. (c) Immunoblots demonstrating the purity of mitochondrial fractions probed with mitochondria-specific anti-COX II antibodies, while anti-RuBisCo and anti-Lhcb1 antibodies serve as negative controls. The target proteins were visualised by HRP-conjugated secondary antibody. (d) Hierarchical clustering of the differentially expressed proteins. The columns represent the dehydration time points, while the rows represent proteins. Heat map shows $\log_2$-transformed expression ratios of 3-day, 6-day, and 9-day dehydration-responsive proteins with respect to those of unstressed control. Higher and lower abundance are indicated by red and blue, respectively. The red asterisk denotes OsDUF2488. (e, f) Venn diagrams representing upregulated (d) and downregulated (e) proteins shared by 3-day, 6-day, and 9-day dehydration. (g) Venn diagram illustrating the overlap of predicted subcellular localisations of the DRPs.

WoLFPSORT. In all, 98 proteins were predicted to be mitochondrial residents (Figure 2g).

The DRPs were classified according to how they participated in various biological processes and molecular functions (Figure S3a, b). The catalogue included proteins mainly with binding, electron carrier, transport and catalytic activities. According to their involvement in biological processes, the majority of the proteins were found to be associated with metabolism and stress response, among others. Next, we compared the rice mitochondrial proteome inventory (Figure S4a, Table S3) with those of other plant species (Bardel *et al*., 2002; Dubinin *et al*., 2011; Jacoby *et al*., 2010; Lee *et al*., 2008, 2011; Salvato *et al*., 2014), which may provide insights into mitochondrial function towards cellular metabolic pathways. Remarkably, comparison with other stress-responsive mitochondrial proteomes previously published revealed distinct and overlapping components (Table S4). The sequence alignment analysis recognised 39 overlapping DRPs, with the remaining as unique dehydration-responsive mitochondrial proteins (Figure S4b, Table S4).

Further, we evaluated to what extent temporal changes in protein expression correlated with the changes in their transcript abundance for randomly selected DRPs (Figure S5a). The log10 transformed values of the differential ratio of protein and transcript abundances were plotted to determine the correlation between proteins and their corresponding mRNA expressions (Figure S5b). The Pearson correlation coefficient ($R = 0.74$) indicates that the protein and transcript abundance followed a linear correlation, albeit the degree of expression varied.

Proteomic identification of dehydration-responsive marker protein OsDUF2488

A critical screening of the proteome enabled us to identify an uncharacterised dehydration-responsive marker, OsDUF2488, harbouring YCF54 or DUF2488 domain. Notably, YCF54-like protein (LOC_Os03g21370) was previously reported in the rice mitochondrial proteome map (Huang *et al*., 2009). Interestingly, OsDUF2488 showed an increased abundance throughout dehydration with a maximal increase at 6 days. The YCF54-like proteins have so far been reported to be associated with chlorophyll biosynthesis in a variety of photosynthetic algae and plants (Chen and Hunter, 2020; Herbst *et al*., 2018; Hollingshead *et al*., 2016). In all, there are 722 YCF54-like proteins in the Pfam database. Localization prediction indicated a number of YCF54-like proteins to be mitochondrial residents [17 by TargetP; 13 by Mitofate; 40 by WoLF PSORT; 13 by iPSORT; 3 by all] (Table S5). Significantly, while MitoProt predicted OsDUF2488 to be localised to the mitochondria, TargetP predicted its location in the chloroplast. To verify the predicted localization of OsDUF2488 in vivo, the expression of OsDUF2488-YFP fusion protein was monitored in Nicotiana epidermal cells. The fluorescence image of OsDUF2488-YFP could be superimposed on the Rhodamine-123-stained fluorescence image of mitochondria and chlorophyll autofluorescence (Figure 3a–f). Importantly, the fluorescence images harbouring Rhodamine-123-stained mitochondria, chloroplast autofluorescence, and OsDUF2488-YFP clearly showed the signals independently from mitochondria (red dotted circle) and chloroplasts (white dotted circle) (Figure 3g). To further confirm the localization of OsDUF2488, immunoblot analysis was performed using specific antibodies with cell lysate, mitochondrial, and chloroplast fractions. OsDUF2488 was found to be predominantly localised to mitochondria, while sparsely to chloroplasts (Figure 3h,i). The enrichment of different fractions was confirmed by the detection of COX II and RuBisCo as mitochondrial and chloroplast marker proteins, respectively.

Nucleotide sequence analysis revealed that OsDUF2488 is located on chromosome 3 of the rice nuclear genome. The genomic size of OsDUF2488 is 3.414 kb with a 621 bp coding region, 132 bp 5′-UTR and 300 bp 3′-UTR. The cDNA encodes a 207 aa protein with a molecular mass of 23.59 kDa and pI 8.95 (Figure 6a). To ascertain the ancestral relationship of OsDUF2488 with its homologues in prokaryotes and eukaryotes, we constructed a phylogram. The homologues were found to be distributed in six distinct clades, wherein those of monocots and dicots clustered separately (Figure 6b).

Stress-induced transcriptional regulation and spatiotemporal expression of OsDUF2488

Consistent with the dehydration-responsive protein expression, OsDUF2488 transcripts were also strongly induced when rice seedlings were exposed to dehydration (Figure 6c). We examined OsDUF2488 expression in response to hypersalinity and oxidative stress since these conditions frequently coincide with the dehydration-responsive pathway. Hypersalinity caused a ~2.5-fold increase in OsDUF2488 transcripts (Figure 6d). Methyl viologen (MV) at sub-lethal doses caused a 100-fold increase in OsDUF2488 expression (Figure 6e), presumably due to the accumulation of superoxide anions and H_2O_2. Also, OsDUF2488 displayed a 2.5-fold increase in response to H_2O_2-induced oxidative stress (Figure 6f). Further, while JA treatment showed a time-dependent increase in OsDUF2488 transcripts up to 4.5-fold at 9 days, a sharp 70-fold increase was observed with SA treatment at 3 days (Figure 6g,h). These results indicate that OsDUF2488 may actively participate not only in abiotic stresses but also in biotic stresses.

It's interesting to note that while expression in other major vegetative organs was comparatively low, OsDUF2488 transcripts were abundant in leaves (Figure 6i). These findings could be significant because organ-specific gene expression is linked to biological substrate flow in vivo within metabolic networks and may be essential for determining agronomic traits.

OsDUF2488 preferentially interacts with OsPrx1.1

To identify proteins that interact with OsDUF2488, yeast-two-hybrid (Y2H) screening was employed. A cDNA expression library was constructed using mRNAs isolated from rice seedlings exposed to 9-day dehydration. The corresponding cDNAs were fused to the GAL4 activation domain to generate the cDNA library. The full-length OsDUF2488 fused to the GAL4 DNA-binding domain (BD) was used as bait. The minimal inhibitory concentration of aureobasidin A (AbA) required for cDNA library screening was 200 ng mL^{-1} (Figure S7a). Screening of the library led to the identification of several putative interacting partners, including a redox protein OsPrx1 (Figure S7b). The interaction of OsDUF2488 with other DRPs was also investigated using the STRING database (http://string-db.org), which recognised 17 DRPs along with OsPrx1 (Figure S8a). Interestingly, both OsDUF2488 and OsPrx1 were found to be upregulated in the dehydration-responsive mitochondrial proteome landscape (Figure S8b,c, Table S2). The sequence analysis revealed two alternative splicing isoforms of OsPrx1, OsPrx1.1 (LOC_Os06g09610.1) and OsPrx1.2 (LOC_Os06g09610.2). Hence, full-length cDNA clones of both OsPrx1.1 and OsPrx1.2 were generated in fusion with the GAL4 activation domain (AD), and the physical interaction was validated with OsDUF2488-BD by Y2H assay (Figure 4a). The Y2H assay

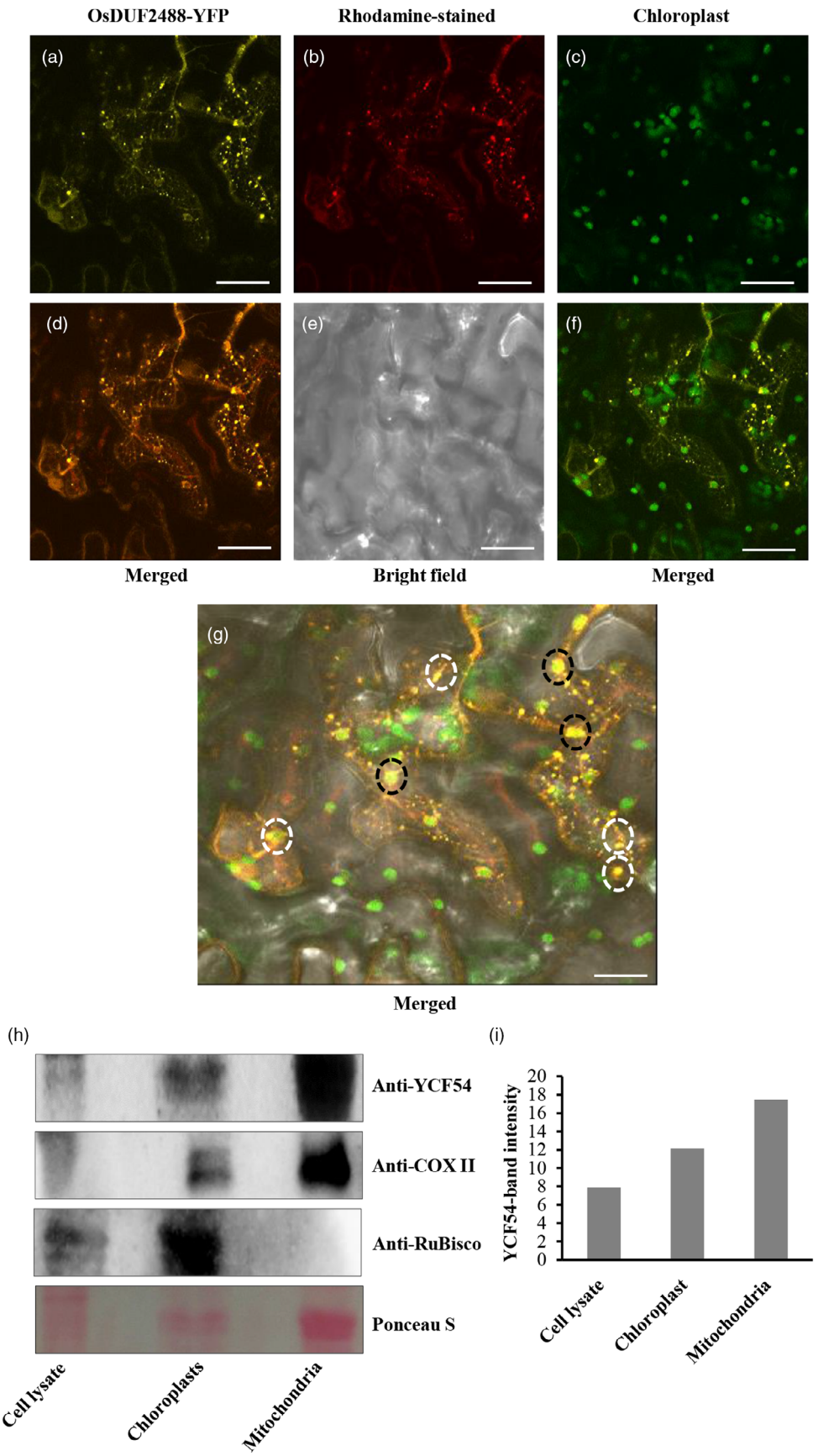

Figure 3 Subcellular localisation of OsDUF2488. (a–f) Confocal microscopy imaging of Nicotiana epidermal cells expressing OsDUF2488-YFP. The fluorescence signals were excited at 488 nm and detected at 500–530 nm. Enhanced yellow fluorescence signals of OsDUF2488-YFP (a), Rhodamine-123-stained mitochondria (b), distribution of chlorophyll autofluorescence (c) and superimposed image of OsDUF2488-YFP and Rhodamine-123-stained mitochondria (d) along with the corresponding bright field image (e). (f) An overlay of the YFP and chlorophyll autofluorescence images. Scale bar, 100 μm. (g) Superimposed image showing fluorescence signals independently from the mitochondria (red dotted circle) and the chloroplasts (white dotted circle). Scale bar, 100 μm. (h) Immunoblot showing differential expression of OsDUF2488 in cell lysate, chloroplasts and mitochondria-enriched fraction isolated from 9-day dehydrated rice seedlings. Proteins were resolved by 12.5% SDS-PAGE, electroblotted onto nitrocellulose membranes and probed with anti-YCF54, anti-COX II and anti-RuBisCo antibodies. Ponceau S staining served as a loading control. (i) The graph represents the quantitative analysis of the bands on the immunoblot.

demonstrated the interaction of OsDUF2488 with OsPrx1.1, but not OsPrx1.2. Additionally, we used a bimolecular fluorescence complementation (BiFC) assay to demonstrate the *in-planta* OsDUF2488-OsPrx1.1 interaction. The fluorescence signals, observed in the mitochondria of cotransformed *Nicotiana* epidermal cells, confirmed that OsDUF2488 and OsPrx1.1 are true interacting partners (Figure 4b). The interaction between OsDUF2488 and OsPrx1.1 was further evaluated by coimmunoprecipitation assay, followed by MS/MS analysis, which authenticated OsPrx1.1 as a bona fide interacting partner (Figure S9a, Table S6). Molecular docking analysis also confirmed the interaction between OsDUF2488 and OsPrx1.1 (Figure S9b,c).

To test the localisation of the isoforms, OsPrx1.1 and OsPrx1.2 were cloned and transformed into rice protoplasts. The confocal images showed that OsPrx1.1 localises to mitochondria (Figure 4c), while OsPrx1.2 localises to the cytosol (Figure 4d).

Overexpression of OsDUF2488 promotes dehydration tolerance and accelerates ROS catabolism

To examine the role of OsDUF2488 in dehydration tolerance, OsDUF2488 was overexpressed in dehydration-sensitive rice cv. IR64 (Choudhary *et al.*, 2009) under the control of the dehydration-inducible promoter, RD29A. Sequence alignment of OsDUF2488 cDNA in cv. IR64 and Rasi showed 100% similarity (Figure S10). In all, 35 independent OsDUF2488-overexpressed (OsDUF2488-OE) lines were confirmed by PCR analysis (Figure 5a). Based on OsDUF2488 expression, three OsDUF2488-OE lines (OE-23-7, OE-28-4 and OE-29-2) were selected for downstream analysis.

To assess and quantify dehydration tolerance, 4-week-old vector transformants and OsDUF2488-OE plants were exposed to dehydration for 13 days, followed by 6-day rehydration. The vector transformants showed severe wilting and chlorosis, with >50% dying of plants at 13-day dehydration (Figure 5b), whereas only a few OsDUF2488-OE plants exhibited dehydration symptoms. The OsDUF2488-OE plants showed significantly higher expression of OsDUF2488 over vector transformants (Figure 5c). Furthermore, the immunoblot analysis using the mitochondria-enriched fraction of OsDUF2488-OE plants showed a severalfold increase in OsDUF2488 expression (Figure 5d). More significantly, the post-recovery survival rate of OsDUF2488-OE plants was markedly higher (>80%) than that of the vector transformants (Figure 5e). To further examine the adaptive responses, the rate of water loss was analysed in detached leaves of vector transformants and OsDUF2488-OE plants. The rate of water loss was faster in vector transformants than that in OsDUF2488-OE plants, indicating that OsDUF2488 might contribute to increased water retention capacity (Figure 5f). The mitochondrial activity of vector transformants and OsDUF2488-OE plants was identical under unstressed conditions, while the transformants showed a significant decrease in ATP concentration and O_2 consumption when exposed to dehydration (Figure 5g,h). To test whether enhanced dehydration tolerance of OsDUF2488-OE plants is contingent on the OsDUF2488-mediated induction of OsPrx1.1, we analysed their expression profiles. Under well-watered conditions, no significant change was observed either in OsDUF2488 or OsPrx1.1 expression in vector transformants and OsDUF2488-OE seedlings. However, the abundance of transcripts was significantly increased when the plants were exposed to dehydration (Figure 5i,j), suggesting OsDUF2488 to be a positive regulator of OsPrx1.1.

The oxidative stress tolerance of OsDUF2488-OE plants was corroborated by the reduced ROS accumulation and lipid peroxidation (Figure 6a). The biochemical analysis further revealed a reduction in MDA and H_2O_2 in OsDUF2488-OE plants (Figure 6b,c). To measure the oxidative stress tolerance, T2 seeds of vector transformants and OsDUF2488-OE plants were plated on MS media supplemented with 0 or 2 μM MV and incubated for 7 days, and tolerance phenotypes were monitored (Figure 6d). The OsDUF2488-OE seedlings exhibited longer roots and shoots ($P < 0.05$) than the vector transformants (Figure 6e). The oxidative metabolic response of OsDUF2488-OE plants was further examined in terms of ROS generation activity by quantifying formazan production. Upon exposure to oxidative stress, formazan production was significantly reduced in OsDUF2488-OE plants compared to vector transformants (Figure 6f).

The transcript abundance of major antioxidants such as APX and catalase was also significantly increased ($P < 0.05$) (Figure 7a–d). To elucidate the systemic changes involved in stress tolerance in OsDUF2488-OE plants, we investigated the transcriptional regulation of SOD isoforms in subcellular compartments. Expression of all three SOD isoforms was enhanced in OsDUF2488-OE plants exposed to dehydration, albeit the increase of cytosolic CuZn-SOD was relatively less (Figure 7e). The peroxidase activity of OsDUF2488-OE plants was also significantly increased under dehydration when compared to vector transformants (Figure 7f). The activation of ROS-scavenging antioxidants strongly suggests that OsDUF2488 might participate in multiple signalling pathways and elicit an integrated stress response. Collectively, these results suggest that OsDUF2488-OE seedlings when exposed to dehydration could quickly enforce ROS-scavenging machinery and help attenuate cell toxicity. Further, we evaluated several agronomic traits of the OsDUF2488-OE plants and the vector transformants, which showed no significant difference in plant height, panicle length and number, grain length and width and seed weight (Figure S11).

OsDUF2488 mutants display enhanced sensitivity to dehydration

To further explore the role of OsDUF2488, rice mutants were generated using CRISPR-Cas9 with two gRNAs targeting exon 2

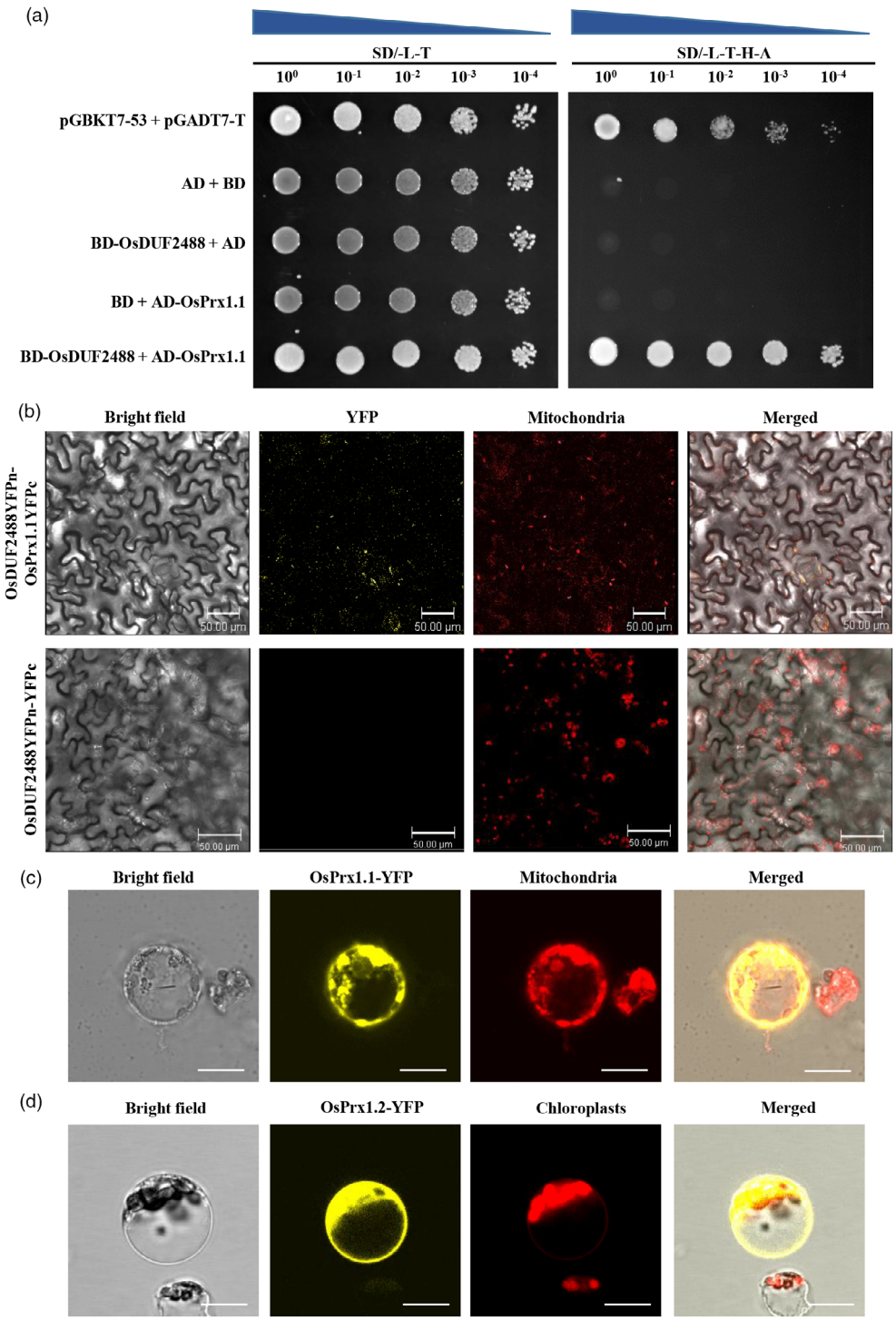

Figure 4 Interaction of OsDUF2488 and localisation of OsPrx1 (OsPrx1.1 and OsPrx1.2). (a) The interaction between OsDUF2488 and OsPrx1.1 was determined by growing the transformants on SD/-Leu-Trp and SD/-Leu-Trp-His-Ade plates supplemented with AbA. Co-transformation with pGBKT7-53 and pGAD7-T served as a positive control, while pGADT7 and pGBKT7 served as negative controls. Confocal microscopy images show the localisation of OsPrx1.1-YFP and OsPrx1.2-YFP in transfected rice protoplasts. (b) *In-planta* interaction of OsDUF2488 and OsPrx1.1 by BiFC in *Nicotiana* epidermal cells. The epidermal cells were transformed with OsDUF2488 and OsPrx1.1 fused with the N- and C-terminal halves of YFP, respectively. The YFP fluorescence signals were observed after incubation at 28 °C for 3 days. Scale bar, 50 μm. (c) Mitochondrial localisation is shown by colocalisation of OxPrx1.1 with the mitochondrion-tracking probe, MitoTracker Red. (d) Overlay images of OsPrx1.2-YFP and chlorophyll autofluorescence. Scale bars, 10 μm.

of OsDUF2488 (Figure S12a). The gRNA expression cassettes were assembled into a CRISPR/Cas9 binary vector (pRGEB32) by Golden Gate ligation (Figure S12b). The editing of the CRISPR vector was checked by transforming it into rice protoplasts followed by sequence confirmation (Figure S12c–e). The vector was transformed into japonica rice through *Agrobacterium tumefaciens*.

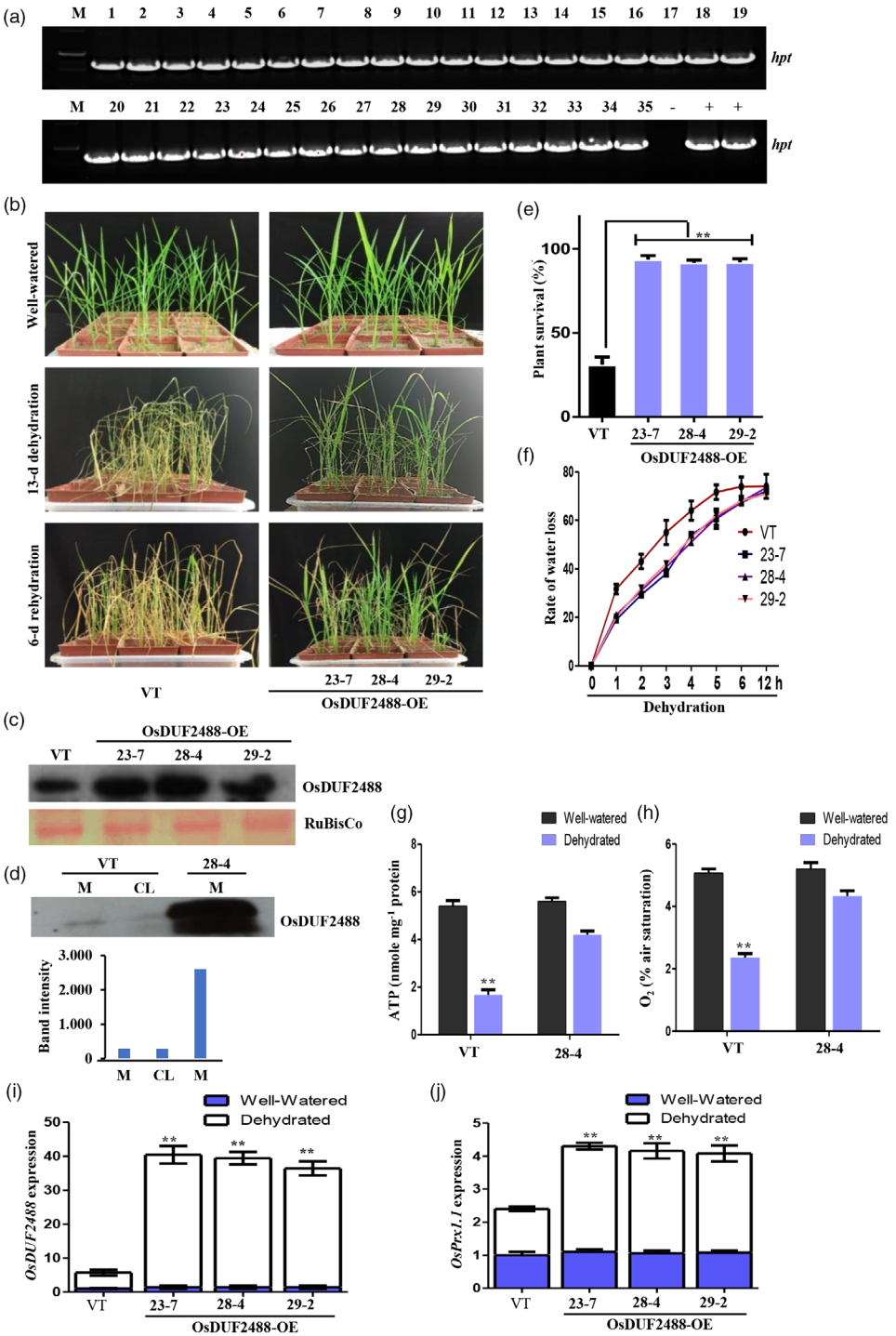

Figure 5 Overexpression of OsDUF2488 in dehydration-sensitive cv. IR64 and evaluation of dehydration tolerance. (a) PCR confirmation of OsDUF2488-OE lines. (b) Dehydration phenotypes of 4-week-old vector transformants (VT) and OsDUF2488-OE plants exposed to dehydration, followed by rehydration as indicated ($n = 3$; eight plants were used in each repeat). (c) Immunoblot showing OsDUF2488 expression in VT and OsDUF2488-OE plants probed with anti-YCF54 antibody. Lower panel corresponds to Ponceau S staining of RuBisCo as a loading control. (d) Immunoblot showing OsDUF2488 expression in cell lysate and mitochondria-enriched fractions of VT, and OsDUF2488-OE plants. The lower panel indicates the band intensity. (e) The survival rate of VT and OsDUF2488-OE plants after rewatering for 6 days. Data represent the mean ± SE of three independent assays with eight plants in each repeat. The asterisks denote a statistically significant difference (*$P < 0.05$, **$P < 0.01$). One-way ANOVA with DMRT post hoc test. (f) Rate of water loss in the detached leaves of VT and OsDUF2488-OE plants up to 12 h ($n = 3$; 10 leaves in each repeat). (g) Mitochondrial ATP production in VT and OsDUF2488-OE plants under well-watered and dehydration conditions. (h) Rate of O_2 consumption in VT and OsDUF2488-OE plants under well-watered and dehydration conditions. Data represent the mean ± SE of three independent assays. The asterisks denote a statistically significant difference (*$P < 0.05$, **$P < 0.01$). One-way ANOVA with DMRT post hoc test. (i, j) Transcript abundance of OsDUF2488 and OsPrx1.1 under well-watered and dehydration conditions. Data represent the mean ± SE of three independent assays with eight plants in each repeat. The asterisks denote a statistically significant difference (*$P < 0.05$, **$P < 0.01$). One-way ANOVA with DMRT post hoc test.

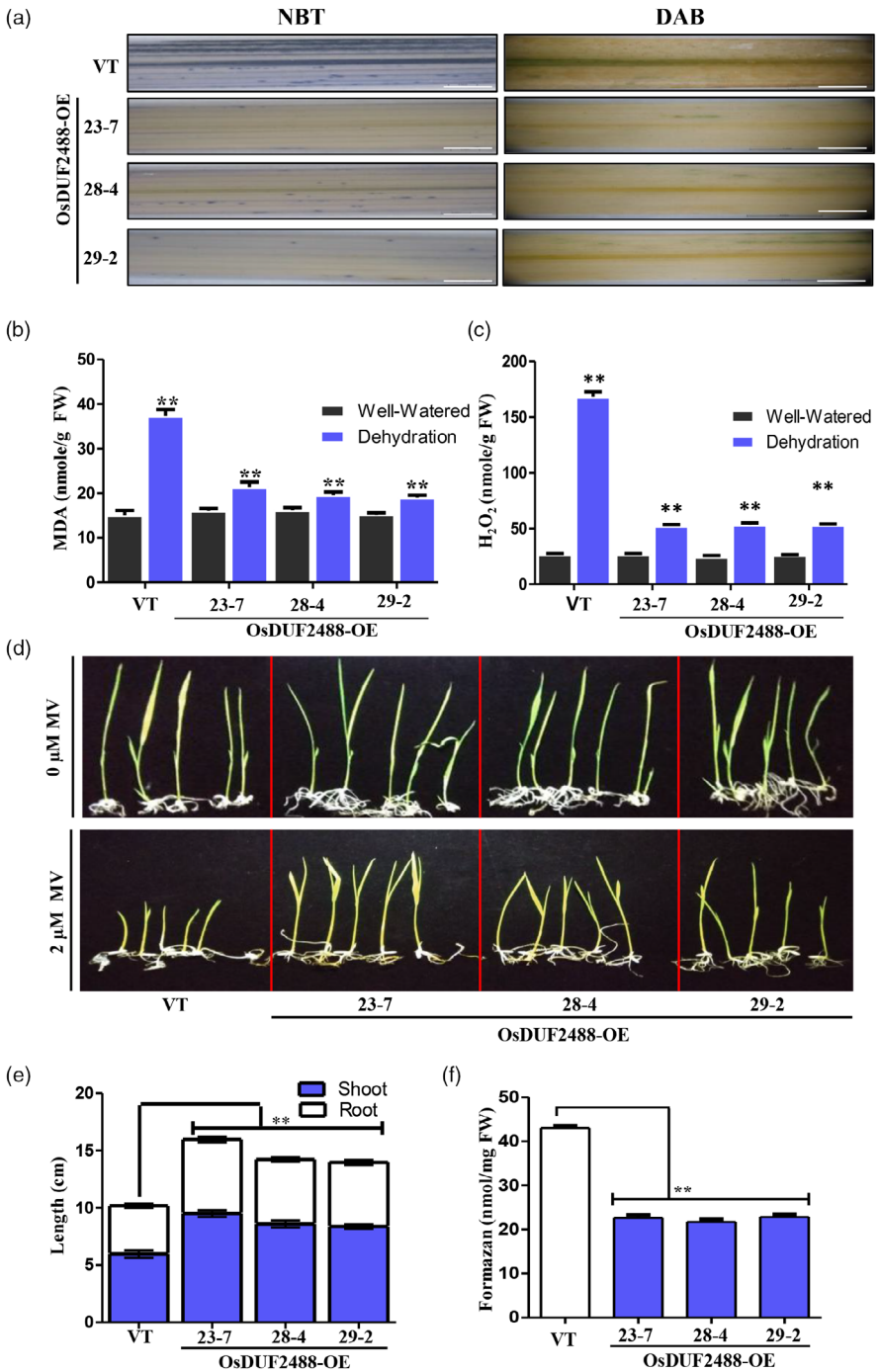

Figure 6 Enhanced ROS catabolism and oxidative stress tolerance. (a) NBT and DAB staining of leaves of vector transformants (VT) and OsDUF2488-OE plants exposed to 9-day dehydration showing the abundance of $O_2^{\cdot-}$ and H_2O_2. NBT, nitroblue tetrazolium; DAB, diaminobenzidine. (b, c) Changes in membrane integrity and lipid peroxidation in terms of MDA and H_2O_2 abundance in VT and OsDUF2488-OE plants. Data represent the mean ± SE of three independent assays with three plants in each repeat. The asterisks denote a statistically significant difference (*$P < 0.05$, **$P < 0.01$). One-way ANOVA with DMRT post hoc test. (d) Oxidative stress phenotype of OsDUF2488-OE plants and VT plated on MS media supplemented with 0 and 2 µM MV for 7 days ($n = 3$; five plants were used in each repeat). (e) Shoot and root lengths of VT and OsDUF2488-OE under MV-induced oxidative stress. Data represent the means ± SE of three experiments (five plants were used in each repeat). **$P < 0.01$, one-way ANOVA with DMRT post hoc test. (f) Reduced formazan concentration in OsDUF2488-OE plants exposed to oxidative stress (MV), indicating low abundance of ROS. Data are representative of three independent experiments and values are expressed in mean ± SE. *$P < 0.05$, **$P < 0.01$, one-way ANOVA with DMRT post hoc test.

Initial screening was conducted using PCR on genomic DNA from the T0 plants to detect the presence of the *SpCas9* gene (Figure S13). In all, 9 Cas9-positive lines were selected for further analysis using target-specific PCR. Since two gRNAs were employed, successful editing was indicated by the presence of two distinct PCR bands, in contrast to the single band observed in

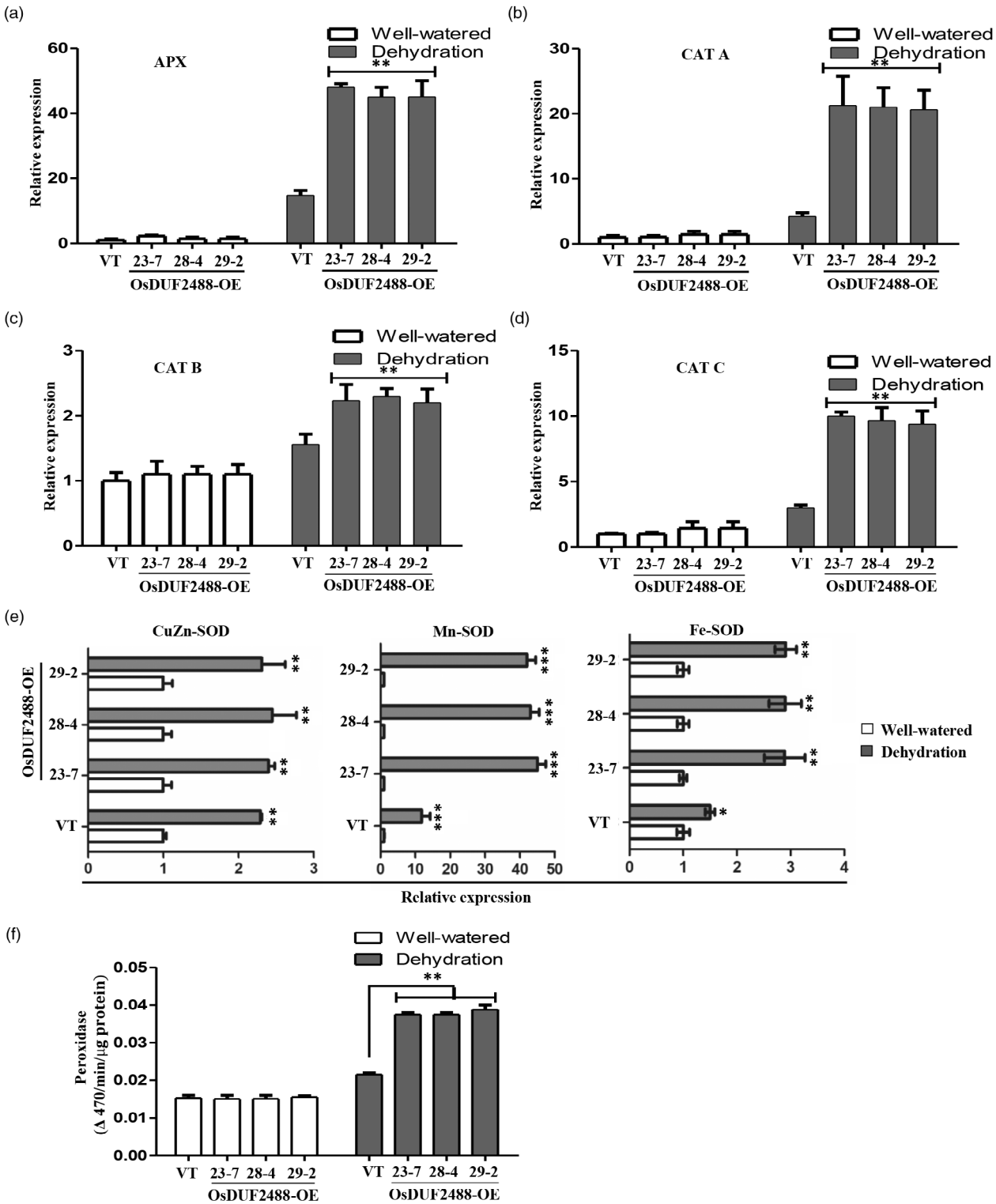

Figure 7 Dehydration-induced transcriptional regulation of ROS-associated genes in OsDUF2488-OE plants and vector transformants (VT). (a–e) Dehydration-induced increased transcript abundance of ROS-associated genes: APX (a), CAT A (b), CAT B (c), CAT C, and various SODs (e). (f) Increased peroxidase activity in OsDUF2488-OE plants exposed to dehydration. Data represent mean ± SE (n = 3). *P < 0.05, **P < 0.01, ***P < 0.001. One-way ANOVA with DMRT post hoc test.

non-transformed controls (Figure 8a). T0 lines exhibiting the expected banding pattern were subjected to Sanger sequencing, which confirmed the intended mutations (Figure 8b). To assess the impact of genome editing, *OsDUF2488* transcript abundance was measured which showed a significant reduction (Figure 8c). T1 plants derived from these lines were re-screened by target-

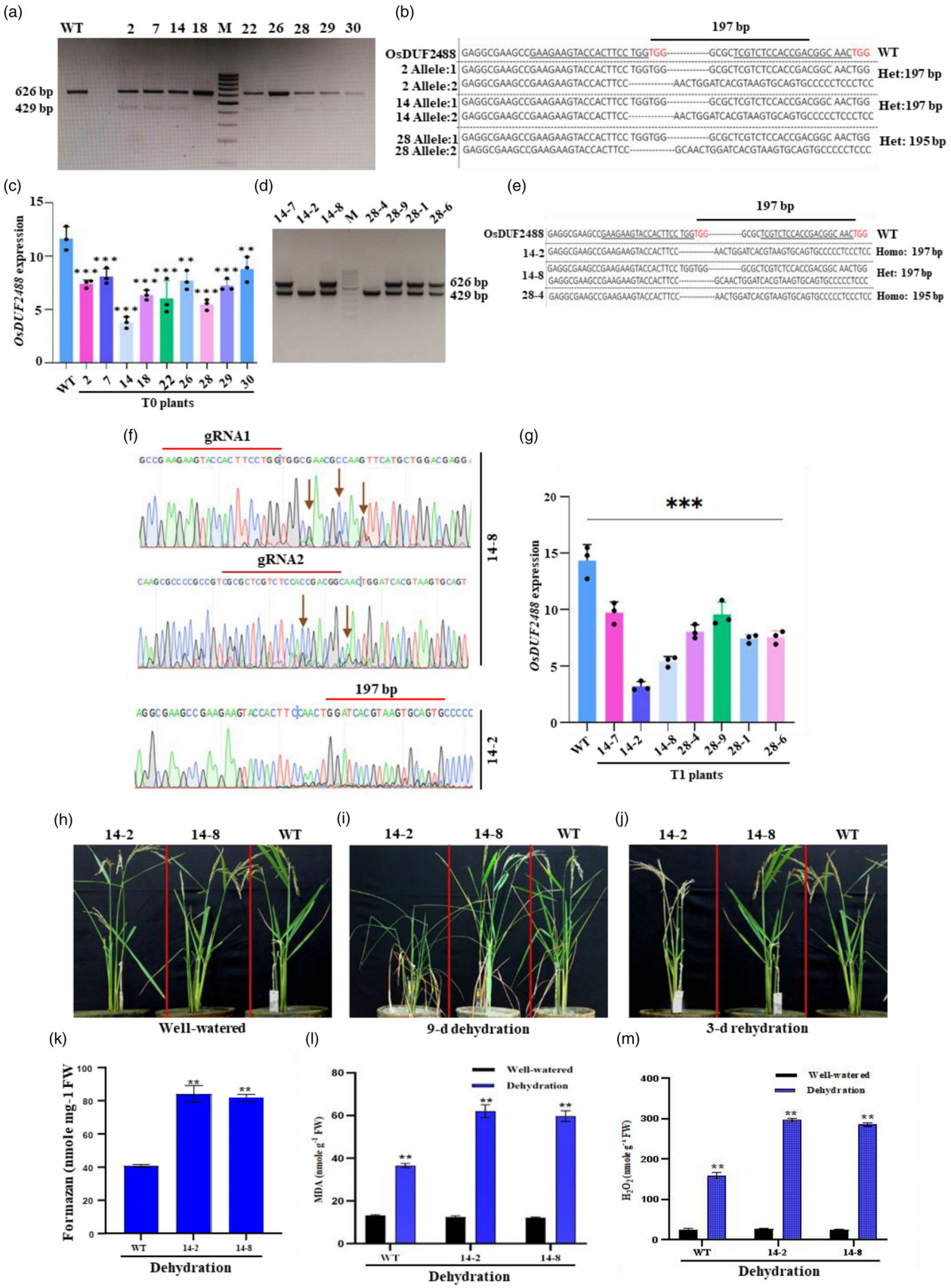

Figure 8 CRISPR-Cas9-mediated mutagenesis of OsDUF2488 in rice and impact on stress tolerance. (a) Amplicons with band size 626 and 429 bp of different T0 mutants, indicating the presence of heterozygous deletions. The numbers represent individual T0 mutant lines. (b) DNA sequence of the T0 edited lines. Black underlined sequence represents the gRNA spacer sequence for the Cas9/gRNA complex, while the PAM sites are shown in red. The deleted nucleotides are depicted by dotted lines. (c) Histogram depicting *OsDUF2488* transcript abundance in T0 mutant lines. Statistical significance is indicated by $^{**}P < 0.01$, $^{***}P < 0.001$. One-way ANOVA with DMRT post hoc test. (d) Amplicons with band size 626 and 429 bp in heterozygous lines, while only 429 bp in homozygous lines of T1 mutants. The numbers represent individual T1 mutant lines. (e) DNA sequence of the T1 mutant lines. Black underlined sequence represents the gRNA spacer sequence for the Cas9/gRNA complex, while the PAM sites are shown in red. The deleted nucleotides are depicted by dotted lines. (f) Sanger sequencing chromatogram of heterozygous mutant (14-8) showing overlapping peaks and homozygous mutant (14-2) indicating deletion of 197 bp. (g) Histogram depicting *OsDUF2488* transcript abundance in T1 mutant lines. Statistical significance is indicated by $^{**}P < 0.01$, $^{***}P < 0.001$. One-way ANOVA with DMRT post hoc test. (h–j) Dehydration phenotype and recovery rate of WT and mutant plants. (k–m) Bar graphs representing reduced formazan concentration (k) and changes in lipid peroxidation in terms of MDA (l) and H_2O_2 abundance (m) in WT and 14-2 and 14-8 mutants exposed to dehydration for 9 days. Data represent the means ± SE of three experiments (five plants were used in each repeat). $^{**}P < 0.01$. One-way ANOVA with DMRT post hoc test. WT, wild-type; M, 100 bp molecular weight marker.

specific PCR and sequencing analysis (Figure 8d–f). The lines showing consistently lower *OsDUF2488* expression compared to non-transformed controls were selected for functional studies (Figure 8g). Two independent mutant lines (14-2 and 14-8) were selected for further analysis. The mutant line 14-2 was homozygous, while 14-8 was heterozygous. Given the potential for off-target effects with CRISPR/Cas9, we used CHOPCHOP to predict the off-target sites in the selected mutant lines. Importantly, no off-target mutations were detected at the analysed sites.

We investigated the impact of mutation by subjecting 4-week-old wild-type and CRISPR/Cas9 mutants to dehydration for 7 days, followed by 3 days rehydration. The results showed higher and lower levels of dehydration sensitivity in 14-2 and 14-8 mutants, respectively, than in the wild-type background. The leaves of 14-2 mutants were more wilted and rolled than those of 14-8 mutants and wild-type plants (Figure 8h–j). More significantly, the rewatered 14-2 mutants remained smaller than the wild-type plants, indicating that the plant growth was inhibited in the mutants by dehydration. After rewatering for 3 days, the degree of recovery from dehydration was greater in the wild-type plants compared with 14-2 and 14-8 mutants. The recovery in wild-type plants was accompanied by a reduction in ROS, MDA, and H_2O_2 levels caused by cellular lipid peroxidation (Figure 8k–m).

OsDUF2488 and OsPrx1.1 act synergistically to confer stress tolerance

To confirm that the OsDUF2488-OsPrx1.1 interaction is fundamental to maintain cellular redox homeostasis and attenuation of stress, we cotransformed OsDUF2488 and OsPrx1.1 into yeast. To this end, full-length cDNA clones of OsDUF2488 and OsPrx1.1 were cotransformed into a yeast strain Y2HGold. The temporal changes in cell growth were monitored under different concentrations of H_2O_2 (0.2–2.0 mM) for wild-type, singly transformed cells (OsDUF2488- and OsPrx1.1-transformants) and cotransformants (Figure 9a). The cotransformants displayed enhanced tolerance compared with that of OsDUF2488- and OsPrx1.1-transformants. In particular, there was a significant reduction in ROS abundance in cotransformants over singly transformed cells (Figure 9b), suggesting that they act synergistically in ROS catabolism. Next, the cells of OsDUF2488-transformants, OsPrx1.1-transformants, and cotransformants were inflicted with dehydration (30% PEG) and hypersalinity (1.25–2.5 M NaCl), and tolerance phenotypes were monitored. The cotransformants showed better survival than OsDUF2488- and OsPrx1.1-transformants, even under stringent stress conditions (Figure 9c–f). These results demonstrate that OsDUF2488 coupled with OsPrx1.1 could maintain redox homeostasis and activate ROS detoxifying machinery, which eventually reverts cellular malfunction.

Discussion

Dehydration-induced changes in mitochondrial proteome dynamics

Rice varieties resilient to water-deficit conditions are rare and thus far, just a few dehydration-resilient cultivars have been identified. To better understand how plants regulate energy metabolism and mount defence against dehydration, we dissected the mitochondrial proteome dynamics of a resistant cultivar of rice. Upon dehydration, different subunits of ATP synthase were found to be upregulated (Table S2), possibly to coordinate continual energy supply for various metabolic processes and cellular adaptations (Lahtvee *et al.*, 2016). Precursors of the ATP synthase were also significantly increased. These results are consistent with a previous report showing upregulation of different subunits of ATPase for stress adaptation (Wang *et al.*, 2015). Yet another set of DRPs associated with the TCA cycle, recognised in the proteome map, included malate dehydrogenase and dihydrolipoyl dehydrogenase (LPD), dihydrolipoyl-lysine-residue succinyltransferase and succinyl-CoA ligase beta-chain (Table S2). The upregulation of mtLPD might lead to increased photosynthetic carbon metabolism, facilitating carbohydrate biosynthesis and branched-chain amino acid degradation and serving as osmoprotectants (Timm *et al.*, 2015). The expression of glutathione S-transferase was downregulated upon exposure to dehydration. Furthermore, prolonged dehydration caused reduced expression of peroxidase precursor, albeit expression of OsPrx1 was increased (Table S2). In plants, Prxs are known to control dithiol-disulfide exchange reaction of target proteins, which modulates redox signalling during stress adaptation (Sevilla *et al.*, 2015). Interestingly, thioredoxin which plays a key regulatory function in plant metabolism (Schurmann and Jacquot, 2000) also displayed high abundance. The mitochondrial transporters such as FtsH protease and mitochondrial-processing peptidase subunit (MPP) were detected as high abundant proteins. Whereas MPP plays a significant role in protein transport (Carrie *et al.*, 2015), FtsH metalloproteases are primarily associated with adaptive responses (Smakowska *et al.*, 2016).

Dehydration-induced translocation of OsDUF2488

A critical analysis of the mitochondrial proteome landscape recognised a dehydration-responsive biomarker, OsDUF2488

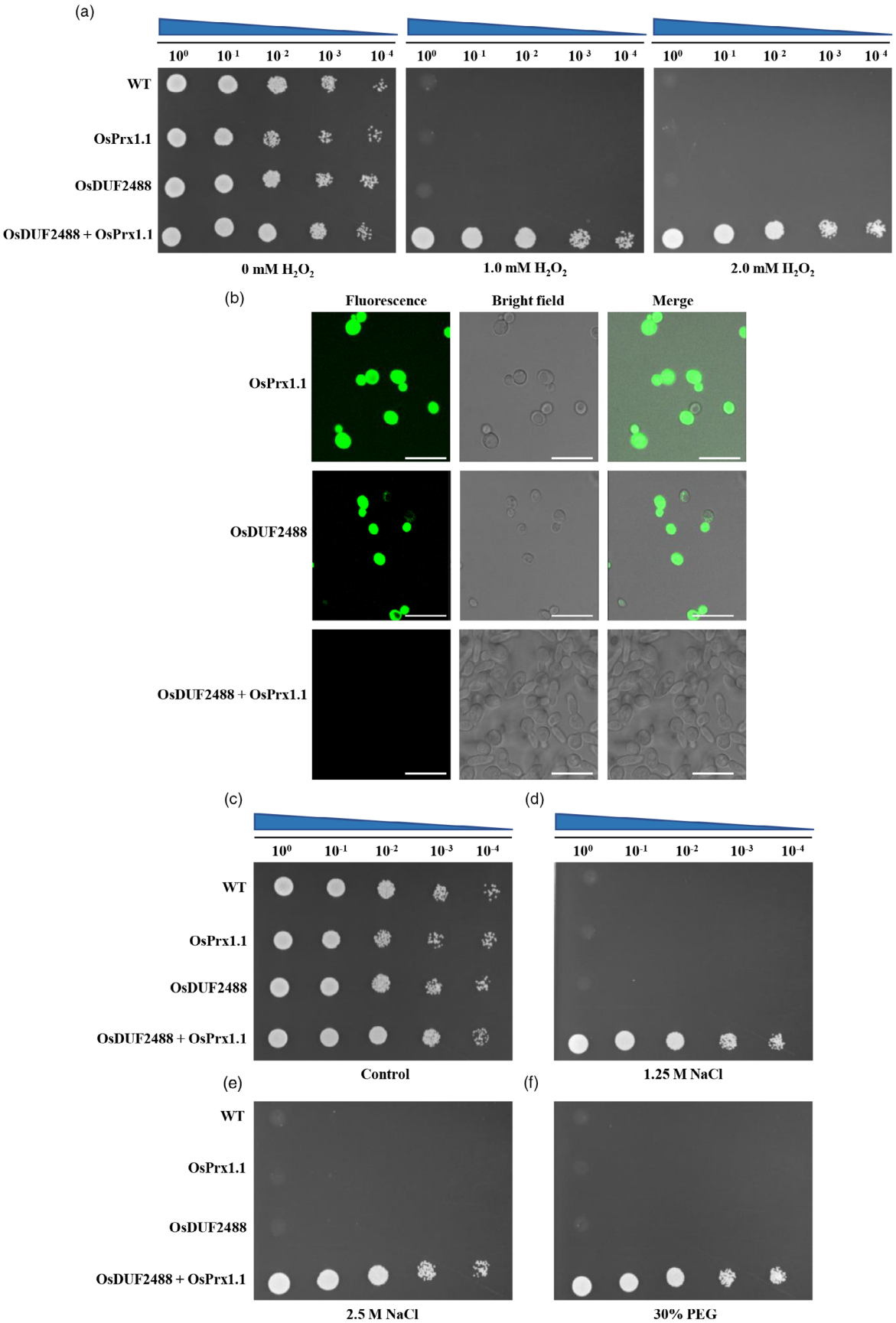

Figure 9 Synergistic effect of OsDUF2488 and OsPrx1.1 in stress adaptation. (a) Yeast growth phenotype (strains transformed independently with OsDUF2488 or OsPrx1.1 or OsDUF2488 + OsPrx1.1) on YPD media (OD_{600} = 0.1) supplemented with various concentrations of H_2O_2 by spot dilution assay. (b) Intracellular ROS production detected by staining with DCFDA at 30 °C for 2 h. The fluorescence was captured under a confocal microscope. Scale bar, 10 μm. (c–f) Relative sensitivity of yeast transformants grown on YPD media supplemented with 1.25 M NaCl (d), 2.5 M NaCl (e) and 30% PEG (f) for 16 h compared to the control condition (c).

(Figure 2d). While investigating the molecular function and physiological significance of OsDUF2488, we verified its subcellular localisation. The YFP-tagged OsDUF2488 showed a distinct overlap with Rhodamine-123-stained mitochondria (Figure 3d). The immunoblot analysis revealed the presence of OsDUF2488 in both mitochondria and chloroplasts (Figure 3h,i). To investigate the dehydration-induced OsDUF2488 abundance in the mitochondria of OsDUF2488-OE plants, immunoblot analysis was carried out using a mitochondria-enriched fraction (Figure 5d). Interestingly, an increased abundance of OsDUF2488 in the mitochondrial fraction suggests that OsDUF2488 might independently play a role as a mitochondrial antioxidant and/or integrate other cellular components, hitherto undiscovered, for an adaptive response.

Mitochondria and chloroplasts are known to evolve parallelly through bacterial endosymbiosis and share similar functions. Over 100 proteins are known to be dually localised to mitochondria and chloroplasts due to protein import mechanisms and signal sequences. Dual targeting of processing peptidase and RADICAL-INDUCED CELL DEATH1 of Arabidopsis has previously been demonstrated (Baudisch and Klosgen, 2012; Shapiguzov *et al.*, 2019). It is increasingly evident that the targeting of proteins, under varied environmental conditions, is facilitated by various mechanisms (Michaud *et al.*, 2010). Notably, YCF54-like protein has previously been reported to be a chloroplast-localised protein, acting as a scaffold protein interacting with the reducing enzyme, ferredoxin-NADPH reductase (Herbst *et al.*, 2018). However, the dual targeting of such proteins in chloroplasts and mitochondria, and the mechanism that provokes their stress-induced translocation to mitochondria are currently unknown and require further investigation.

Stress-responsive regulation of OsDUF2488

The available rice bioinformatics resources suggested that the YCF54-like proteins are regulated by various developmental and environmental cues (Jain *et al.*, 2007; Lasanthi-Kudahettige *et al.*, 2007). Since spatiotemporal regulation of gene expression is an important signature, we quantified the abundance of OsDUF2488 in various tissues/organs, which showed the highest expression in leaves over other organs (Figure S6i).

The transcripts of OsDUF2488 were also significantly induced under dehydration and oxidative stress (Figure S6c,e). Hence, the effect of oxidative stress on the expression of OsDUF2488 was investigated using two different oxidising agents, MV and H_2O_2. While MV catalyses ROS production from the electron transport chain, which represents organelle-generated ROS, H_2O_2 functions as exogenous ROS, affecting direct cellular oxidative stress (Li *et al.*, 2013). Emerging evidence suggests that energy-converting organelles, chloroplasts and mitochondria, produce toxic levels of ROS at high concentrations of MV (Cui *et al.*, 2019). In the acceptor side of chloroplast PSI, MV radical cations are formed by interaction with O_2 and produce superoxides (Aguiar *et al.*, 2023). In non-photosynthetic organisms, MV-driven mitochondrial ROS production is caused by transferring electrons from NAD(P)H (Cocheme and Murphy, 2008). Previous studies in Arabidopsis demonstrated that both chloroplasts and mitochondria participate in ROS production (Cui *et al.*, 2019). Therefore, the striking increase in OsDUF2488 transcripts with MV treatment (Figure 6e) conclusively suggests that OsDUF2488 may have a crucial role in ROS catabolism and maintenance of cellular redox status.

OsDUF2488 and OsPrx1.1 synergistically enhance stress tolerance

It is widely recognised that ROS plays a crucial role in cell signalling in a series of biological processes, while excess ROS causes severe cellular damage (Zhou *et al.*, 2018). In this study, we demonstrated an interaction between OsDUF2488 and OsPrx1.1 (Figure 3, Figures S8a and S9), implying a synergistic antioxidant activity. Among the key detoxifying enzymatic antioxidants, Prxs constitute a very specialised group of thiol-dependent peroxidases, and are ubiquitously present in almost all organisms (Cox *et al.*, 2010; Dietz, 2011). More significantly, Prxs are most abundant in plants compared to other organisms for ROS homeostasis, particularly produced during photosynthesis. The Prxs are classified into four functional subgroups: PrxQ, 1-CysPrx, 2-CysPrx and Type-II Prx. To date, the genome-wide analysis identified 10 Prxs in rice, albeit only one has been functionally characterised (Gho *et al.*, 2017). Among the Prxs, PrxQ is involved in the regulation of cold and hypersalinity stress responses (Jing *et al.*, 2006).

Sequence alignment analysis indicated that OsPrx1 has homology with rice PrxQ (Table S6), which is not yet characterised. The Prxs were previously reported to be chloroplast-residing proteins by several independent groups (Lamkemeyer *et al.*, 2006; Rouhier *et al.*, 2004). We conclusively demonstrated the molecular interaction between OsDUF2488 and OsPrx1.1 (Figure 3, Figures S8a and S9). We propose that the OsDUF2488-OsPrx1.1 interaction is crucial for the maintenance of redox homeostasis, which may play a key role in antioxidant defence. Significantly, the coexpression of OsDUF2488 and OsPrx1.1 in yeast confirmed the proposed linkage between OsDUF2488-mediated OsPrx1.1 induction and ROS catabolism (Figure 9).

OsDUF2488 improves dehydration tolerance in rice

Overexpression of OsDUF2488 in dehydration-sensitive cv. IR64, under the RD29A promoter, was able to drive its dehydration-mediated expression and could avoid pleiotropic effects usually exerted by constitutive promoters. The OsDUF2488-OE plants exhibited improved dehydration tolerance with enhanced antioxidant capacity (Figures 5b–j and 6a–f). Contrastingly, the mutant plants exhibited more sensitivity to dehydration and showed oxidative damage and growth inhibition (Figure 6e–h). When exposed to dehydration, the transcripts of both OsDUF2488 and OsPrx1.1 were increased severalfold in OsDUF2488-OE plants (Figure 5i,j), suggesting that OsDUF2488 might act as a positive regulator of OsPrx1.1. The transcript abundance of several ROS catabolising enzymes viz., APX, catalase, and SOD was also

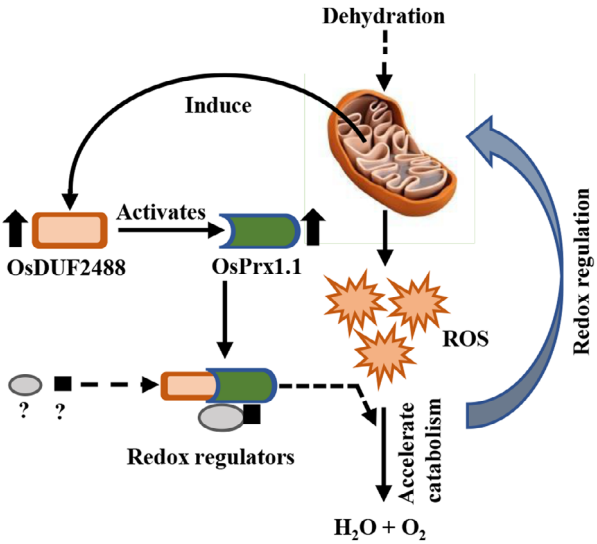

Figure 10 Predicted redox homeostasis involving OsDUF2488. Dehydration-induced perturbation of mitochondrial redox homeostasis promotes mtROS accumulation, causing oxidative damage. One of the intricate strategies that repress mtROS production is orchestrated by increased expression of OsDUF2488. OsDUF2488 interacts with and activates OsPrx1.1 and forms a redox-complex with yet-to-be-identified regulators. This regulatory complex accelerates mtROS catabolism and rescues mitochondrial dysfunction. The question marks represent unidentified regulatory proteins. Upward arrows indicate upregulated expression.

induced by OsDUF2488 expression (Figure 7). This corroborates the findings of several earlier studies, displaying enhanced tolerance by improved ROS catabolism and high expression of ROS-scavenging enzymes (Li *et al.*, 2023; Xu *et al.*, 2023).

In general, plants develop dehydration resiliency through avoidance, tolerance, and recovery (Bhushan *et al.*, 2007). While dehydration avoidance is achieved by reducing water loss, the tolerance mechanism is established by adjustment of osmotic and antioxidant capacities. Here, we demonstrated that OsDUF2488 primes the ROS catabolism process in OsDUF2488-OE plants exposed to dehydration and oxidative stress with no effect either in vector transformants or OsDUF2488-OE plants under unstressed conditions (Figures 5 and 6). In conclusion, this study recognised the dehydration-induced mitochondrial translocation of a YCF54-like protein, OsDUF2488. Investigation on the role of OsDUF2488 in stress tolerance revealed that OsDUF2488 interacts with OsPrx1.1, and the interaction is critical for the regulation of adaptive responses. There was a synergistic interaction effect on ROS catabolism in yeast, while OsDUF2488-induced expression of OsPrx1.1 and other ROS catabolising enzymes was evident in both mitochondria and chloroplasts. We propose that besides the well-known function of YCF54-like proteins in chlorophyll biosynthesis, OsDUF2488 might be involved in the induction of mitochondrial OsPrx1.1 and play a role in ROS homeostasis (Figure 10). It may also function in the reduction of mitochondrial ROS production by upregulation of mitochondrial SOD and other ROS-scavenging pathways. Dehydration tolerance being a complex polygenic trait, attempts to improve such traits through conventional breeding have had limited success. Alternatively, the identification of potential protein markers that confer resiliency to dehydration through transgenic technology is often projected as one of the sustainable crop protection solutions. Overall, our findings indicate that OsDUF2488 is highly promising for engineering improved stress tolerance in crops in general and rice in particular.

Experimental procedures

Seedling growth and stress treatments

The seedlings of rice (*Oryza sativa* L. cv. Rasi) were raised in a plant growth chamber (Choudhary *et al.*, 2009). Four-week-old seedlings were subjected to dehydration by withholding water, and samples were collected at 3-day intervals for 9 days. The quantitative proteomic analysis was performed with unstressed control and 3-day, 6-day, and 9-day dehydrated tissues. In a separate set of experiments, for determining transcript abundance, the seedlings were exposed to various stress conditions and phytohormone treatments: (i) hypersalinity (200 mM NaCl) and sampled at 0, 3, 6, and 12 h; (ii) oxidative stress by foliar spray, independently with 300 mM H_2O_2 and 2 μM MV, and sampled at 0, 1, 3, and 6 h; (iii) foliar spray with SA (100 μM) and JA (100 μM) and sampled at 0, 1, 3, 6, and 12 h.

Analysis of physicochemical indexes and mitochondrial ultrastructure

Leaf RWC was determined following the method described earlier (Choudhary *et al.*, 2009). SMC was determined by the oven drying method. A portable photosynthesis system (LI-6400, Li-Cor Inc.) was employed to analyse the photosynthetic rate, stomatal conductance and intercellular CO_2 concentration under a saturating partial pressure flow rate (PPFD) of 1500 mol m^{-2} s^{-1}. Relative humidity was kept at 20%, and the ambient CO_2 concentration in the cuvette (Ca-c) was adjusted to match the atmospheric CO_2 concentration (416 ± 1.5 μmol CO_2 mol^{-1}). Data were recorded after equilibration for 10 min to a steady state condition (Li *et al.*, 2009). The H_2O_2 concentrations were measured using fluorescence dye 2′,7′-dichlorofluorescin diacetate (DCFDA) at Ex-495 nm/Em-529 nm, and the resulting values of ROS were expressed by relative fluorescent intensity per g FW. The concentrations of MDA and proline were determined as previously described (Bhushan *et al.*, 2007).

Mitochondrial morphology was determined using a transmission scanning electron microscope (JEOL 2100F) under low vacuum mode at 5 °C involving 133.32 Pa pressure and 5 kV voltage. Paraffin-embedded tissue samples (unstressed control and 3-day, 6-day and 9-day dehydrated) were sliced into ultrathin (5-μm-thick) sections and processed as previously shown (Gayen *et al.*, 2019).

Enrichment of mitochondrial fraction and extraction of proteins

Intact mitochondria were isolated from unstressed control and dehydrated tissues by the method described earlier (Gayen *et al.*, 2019). The integrity of the mitochondrial membrane was evaluated by cytochrome c oxidase (50 μg/mL) activity at 550 nm with and without Triton X-100 (0.05% (w/v)) (Moller *et al.*, 1987). The mitochondrial proteins were extracted using acetone and then centrifuged at 20 000 ***g*** for 15 min. The protein pellet was ultrasonically dissolved in 7 M urea, and a 3 kDa column was used to exchange the buffer with 0.5 M TEAB. The protein extracts were centrifuged at 15 000 ***g*** for 10 min, and the supernatant was retrieved for downstream analysis. The protein

concentrations were determined by BCA protein assay (Thermo Fisher Scientific).

Immunoblot analysis

Immunoblotting was carried out by resolving 50 μg proteins onto 12.5% SDS-PAGE, followed by electrotransfer onto a nitrocellulose membrane for 2 h at 150 mA. The membranes were blocked with 5% (w/v) non-fat milk for 16 h and incubated with the target primary antibodies (anti-COX II, Agrisera A S04 053A; anti-RuBisCo, Agrisera AS03 037; anti- Lhcb1, Agrisera AS01 004 and anti-YCF54, Agrisera AS10936anti-YCF54) for 2 h at room temperature. The blots were then incubated with HRP-conjugated secondary antibody (Agrisera AS09 602) for 1 h, and then the signals were detected using an ECL substrate (Bio-Rad Laboratories).

Protein digestion, iTRAQ-labelling and mass spectrometry

The in-solution digestion and iTRAQ-labelling were performed as previously described (Gayen *et al*., 2019). In brief, 100 μg mitochondrial proteins from unstressed control and dehydrated (3, 6 and 9 days) tissues were digested with trypsin at 37 °C. The digested peptides were labelled with iTRAQ 4-plex kit according to the manufacturer's instructions (AB Sciex) as depicted in Figure S1. The iTRAQ-labelled peptides were suspended in solvent A (10 mM ammonium formate, pH 10) and fractionated by HPLC (1260 Infinity, Agilent Technologies). The eluted fractions were dried and dissolved in 2% ACN, 0.1% formic acid. The proteins were identified on a TripleTOF 5600 system (AB Sciex) connected to NanoLC. The samples were separated with a gradient run (300 nL/min) from 5% buffer B (0.1% formic acid in ACN) to 90% buffer B. The mass spectrometer settings varied for the analysis depending on optimisation, but typical values were: curtain gas 25, an ion spray floating voltage around 2000–2300 V and heater interface temperature of 130 °C. The analysis was done with an information-dependent acquisition mode, and each cycle consisted of a TOF MS survey scan of 250 ms covering m/z 350–1250. A maximum of 20 precursor ions per cycle were selected for fragmentation, and each MS/MS spectrum (100–1600 m/z) was accumulated for 100 ms with a total cycle time of approximately 2.3 s. The recalibration of the mass spectrometer was performed for each sample using a β-galactosidase standard. Protein identification and quantification were carried out using the ProteinPilot software (v 4.5; AB Sciex) employing the Paragon algorithm. The search parameters were: (i) sample type, iTRAQ 4-plex (peptide-labelled); (ii) cysteine alkylation, methyl methanethiosulfonate (MMTS); (iii) digestion, trypsin; (iv) instrument, TripleTOF 5600; (v) special factors, none; (vi) species, *Oryza sativa* and (vii) database, NCBInr.fasta (protein sequence). Proteins were identified with 1% FDR, and the results were exported to Excel for manual data interpretation.

RNA extraction and RT-qPCR analysis

Total RNAs were isolated by TRIzol reagent. The reverse transcription reaction (SuperScript III First-Strand Synthesis System, Invitrogen) was performed with 5 μg RNA, and the transcripts were analysed (ABI Prism 7700 Detection System, Applied Biosystems) using Power SYBR Green PCR Master Mix with gene-specific primers (Table S7). β-tubulin was used as an internal control for the normalisation of gene expression.

Enzyme activity assay

The activity of cytochrome c oxidase was determined by decreasing the absorbance of ferrocytochrome c (21 mM^{-1} cm^{-1}) at 550 nm caused by its oxidation to ferricytochrome c (Moller *et al*., 1987). The rate of decrease in absorbance was measured every minute, and the activity was calculated with an extinction coefficient of 21.84. Peroxidase activity was calculated with the increasing absorbance of tetra-guaiacol at 470 nm (Castillo *et al*., 1984). The enzyme activity was estimated as per the extinction coefficient of its oxidation product, tetra-guaiacol $\varepsilon = 26.6$ mM^{-1} cm^{-1}. The reaction mixture (3.0 mL) included 50 mM phosphate buffer (pH 6.1), 16 mM guaiacol, 2 mM H_2O_2 and 0.1 mL plant extract.

Subcellular localisation in Nicotiana epidermal cells and rice mesophyll protoplasts

The full-length cDNA of OsDUF2488 and OsPrx1.1 and OsPrx1.2 was amplified by PCR using gene-specific primers (Table S7), and independently cloned into the pENTR vector. The OsDUF2488 was subcloned into pGWB441. The construct and the empty vector were transformed via Agrobacterium tumefaciens strain GV3101. The transformed strains were then grown in a YEP medium supplemented with rifampicin (50 μg/mL) and kanamycin (50 μg/mL) at 28 °C for 20 h while being constantly shaken. The cells were collected by centrifugation, and resuspended in the infiltration buffer (10 mM $MgCl_2$, 10 mM MES, and 200 μM acetosyringone, pH 5.7). The transformed cells were introduced into the leaves of 4-week-old Nicotiana seedlings and allowed to grow at 25 °C for 48 h.

To determine the localisation of OsPrx1.1 and OsPrx1.2, the respective cDNAs were subcloned into pSITE-3CA. The fusion constructs were transfected into rice mesophyll protoplasts as previously described (He *et al*., 2016). Transformation of protoplasts was performed using the PEG-CaCl2 method. The protoplasts were mixed with the fusion constructs (>5 μg) in 2-mL microcentrifuge tubes at a concentration of ~1 μg/μL. Then, 100 μL PEG-$CaCl_2$ solution (40% PEG 4000, 0.2 M mannitol, 100 mM $CaCl_2$, pH 5.7) was added and mixed by tapping. After 20 min of incubation at 25 °C, transfection was stopped by adding 1 mL W5 solution and gently inverting several times. The transfected protoplasts were collected by centrifugation at 1000 ***g*** for 5 min and suspended in 1 mL W1 solution (0.2 m MES, 0.5 M mannitol, 20 mM $MgCl_2$, pH 5.7), and incubated 12–14 h at 25 °C. The Nicotiana epidermal cells and rice protoplasts transfected with respective OsDUF2488-YFP, OsPrx1.1-YFP, and OsPrx1.2-YFP fusion constructs were examined by fluorescence confocal microscopy (TCS-SP8, Leica).

Construction of Y2H library and screening

Yeast two-hybrid library was prepared using Matchmaker GAL4-based two-hybrid system (Clontech) as per manufacturer's protocol. The cDNAs were amplified from 9-day dehydrated tissues and then transformed with pGADT7-Rec vector in yeast Y187 cells. The library was screened with OsDUF2488 as bait and the transformants were selected on high stringency (SD/-Ade/-His/-Leu/-Trp/X-α-Gal/AbA) plates. The positive interaction was confirmed by cloning the full-length cDNAs of OsPrx1.1 and OsPrx1.2 into pGADT7 and co-transformation with BD-OsDUF2488 construct, followed by selection on SD/-Leu/-Trp and SD/-Ade/-His/-Leu/-Trp media.

BiFC assay

The cDNAs of *OsDUF2488* and Os*Prx1.1* were independently cloned into the pENTR-D-Topo vector (Invitrogen). The cDNAs were then introduced into the gateway vector pSITE-nEYFP-C1 (ABRC stock number CD3-1648) or pSITE-cEYFP-N1 (ABRC stock number CD3-1651), respectively. The recombinant vectors encoding nEYFP-OsDUF2488 and cEYFP-OsPrx1.1 were transformed into Agrobacterium, followed by co-transformation into *Nicotiana* epidermal cells. The cotransformed cells were incubated at 28 °C for 3 days, and YFP signals were detected by confocal laser scanning microscopy.

Coimmunoprecipitation assay

Coimmunoprecipitation was performed using the Dynabeads Protein G coimmunoprecipitation kit (Thermo Fisher Scientific). The anti-YCF54 (Agrisera AS10936) was covalently coupled to magnetic Dynabeads G (1.5 mg), following the manufacturer's instructions. Approximately 6 mg protein, extracted from rice seedlings exposed to dehydration, was added to the bead-antibody complex and incubated for 10 min. After washing, the IP products were eluted with elution buffer (pH 2.8). An aliquot of the eluted proteins was analysed through SDS-PAGE and immunoblotting, while the rest were used for identification by MS/MS analysis.

Overexpression of OsDUF2488 in rice and assay of stress tolerance

The full-length OsDUF2488 cDNA from cv. Rasi was amplified using gene-specific primers (Table S7) and confirmed by sequence analysis. The 621-bp amplicon was subcloned into the polylinker site BamHI-KpnI of the binary vector pCAMBIA1301. The recombinant vector, pCAMBIA-RD29A-OsDUF2488-nos, was introduced into rice cv. IR64 by Agrobacterium-mediated transformation (Karmakar *et al.*, 2016). The sterilised dehusked seeds were incubated at 30 °C for 14 days in callus-inducing media (CIM) supplemented with N6 basal salts and 2,4-D. The freeze–thaw technique was used to transform the Agrobacterium strain LBA4404. The transformed strains were cultured at 28 °C for 48 h, pelleted down, and resuspended in liquid CIM containing 100 mM acetosyringone. The transformed cells were introduced into 14-day-old embryogenic calli. Following a 72-h co-cultivation period, the infected calli were rinsed with liquid CIM containing 200 mg/L timentin. Next, the calli were incubated in selection media supplemented with 50 mg/L hygromycin and 200 mg/L timentin for 21 days. The calli were then transferred to regeneration media, and the regenerated plantlets were acclimatised in the greenhouse. The putative overexpressed plantlets were screened by PCR amplification of the hygromycin and OsDUF2488 genes.

The biochemical and molecular indices of OsDUF2488-OE lines were compared with those of vector transformants. The sterilised seeds of OsDUF2488-OE lines and vector transformants were germinated on ½-MS medium under a 14-h light (28 °C)/10-h dark (25 °C) photoperiod for 5 days. The germinated seedlings were then subjected to oxidative stress by transferring to ½-MS media containing 2 μM MV for 6 days. In a separate set of experiments, 4-week-old OsDUF2488-OE seedlings and vector transformants were exposed to dehydration by withholding water for 13 days, followed by rehydration for 6 days. Leaf $O_2^{\cdot-}$ and H_2O_2 were estimated by NBT and DAB staining (Kaur *et al.*, 2016). The formazan content of NBT-stained seedlings was measured by dissolving in DMSO as previously described (Bournonville and Diaz-Ricci, 2011). The rate of water loss was determined as described elsewhere (Wang *et al.*, 2018).

Analysis of mitochondrial O_2 consumption rate and ATP synthesis

The mitochondrial respiratory O_2 consumption of unstressed control and dehydrated OsDUF2488-OE seedlings and vector transformants was measured using a TBR1025 single-channel free radical analyser (World Precision Instruments, Sarasota, FL). ATP content was measured by a luciferase-based assay using 250 ng protein as described previously (Gayen *et al.*, 2019). The mitochondrial ATP was extracted by 10% TCA and centrifuged at 10 000 ***g*** for 5 min at 4 °C. The supernatant was neutralised with 10 M KOH followed by centrifugation at 10 000 ***g*** for 5 min at 4 °C. The neutralised supernatant was used for ATP content by an ATP determination kit (Molecular Probes).

Transformation of yeast and assessing cell survival

Both OsDUF2488 and OsPrx1.1 were cotransformed into a yeast strain Y2HGold (G-Bioscience). The temporal changes in yeast cell growth were monitored under different concentrations of H_2O_2 (0.2–2.0 mM) as previously described (Tran and Green, 2019) for 1 h. The stimulated production of ROS was visualised by staining with DCFDA dye followed by confocal microscopic imaging.

CRISPR/Cas9-mediated mutation of OSDUF2488 in rice

The gRNA sequences were designed using the online CRISPR-GE tool (Ma *et al.*, 2015) based on the genome sequence of OsDUF2488 in rice (japonica group, cv. Kitaake; 03g166100_DUF2488) located on chromosome 3. The CRISPR-GE tool provided the possible list of gRNA sequences within the specific genomic context based on the protospacer adjacent motif (PAM). The potential target of 20 nucleotides located immediately upstream of the PAM site at 3′ was selected. Two gRNA sequences were selected based on the respective GC percentage and absence of multiple T nucleotides in the corresponding target sequence. The secondary structure of gRNA was analysed using an RNAfold web server. We designed a polycistronic tRNA-gRNA (PTG) cassette to target exon 2 of OsKitaake03g166100_-DUF2488 as previously described (Xie *et al.*, 2015). To increase the editing efficiency, the tRNA sequence was fused upstream of every gRNA. Three fragments [PS1 (128 bp), PSII (195 bp) and PSIII (138 bp)] for two gRNAs were assembled using Golden Gate cloning. The assembled segments were ligated into the pGEMT-easy vector and confirmed by Sanger sequencing. The completed segment was subcloned into pRGEB32 under the control of the OsU3 promoter.

The on-target efficiency was examined using rice protoplasts transfected with the above-mentioned construct. Genomic DNA was extracted from the transfected protoplasts using the NucleoSpin Plant II kit (Takara Bio). The genomic region targeted by the gRNA was amplified using two sets of primers (DUF2488-F and DUF2488-R) (Table S7). The purified PCR products were confirmed by Sanger sequencing. The targeted gene mutations were validated by interpreting the sequencing chromatograms of the amplicon with the wild-type using the SNAPGENE software. Next, the CRISPR/Cas9-targeted mutation in rice was carried out by Agrobacterium-mediated transformation (Karmakar *et al.*, 2016), and the mutants were validated as described above. To detect the off-target sites, each gRNA sequence was analysed using the online CHOPCHOP tool (https://chopchop.cbu.uib.no/)

with the *Oryza sativa* (Kitaake v3.1) genome as the reference. The off-target loci were amplified with specific primers (Table S8), followed by Sanger sequencing to detect any unintended mutations.

Statistical analysis

The ProteinPilot™ software (AB Sciex) was used for protein identification and quantification. The software performs automated data normalisation and statistical evaluation of peptide/protein ratios using built-in algorithms based on confidence scores and Bayesian models. For subsequent downstream statistical analysis using one-way ANOVA, the processed iTRAQ quantification data were exported. To stabilise variance and improve normality, the iTRAQ ratio data were log2-transformed prior to downstream analysis. GraphPad Prism v7.0 was used for all statistical and graphical analyses. One-way ANOVA was conducted to assess differences between experimental groups, followed by Duncan's Multiple Range Test (DMRT) as a post hoc analysis to identify statistically significant differences among OsDUF2488-overexpressing, OsDUF2488-knockout seedlings and vector control transformants, as well as among other datasets. Statistical significance was denoted as $*P < 0.05$, $**P < 0.01$ and $***P < 0.001$.

Accession numbers

OsDUF2488 (LOC_Os03g21370), OsPrx1.1 (LOC_Os06g09610.1) and OsPrx1.2 (LOC_Os06g09610.2).

Acknowledgements

This work was supported by grants (BT/184/NE/TBP/2011) from the Department of Biotechnology (DBT), Govt. of India, the Indian National Science Academy (INSA), New Delhi and the BRIC-National Institute of Plant Genome Research, New Delhi to N.C. We also acknowledge the financial support from the Science and Education Research Board (SERB, Govt. of India) for the post-doctoral fellowship (PDF/2016/002615) to D.G. We thank Mr. Jasbeer Singh for illustrations and graphical representation in the manuscript.

Conflict of interest

The authors declare no competing financial interests.

Author contributions

N.C. conceived and directed the research. D.G., S.K. (Sunil Kumar), P.B., and N.V.L. designed and performed the experiments. A.K.D. and T.K.M. contributed to mass spectrometry. S.K. (Subhasis Karmakar) and K.A.M. helped in genome editing experiments, and S.M. in *in-planta* interaction assay. D.G., S.K. (Sunil Kumar), P.B., N.V.L., S.G., S.C., and N.C. processed the experimental data and performed analyses. D.G., S.K. (Sunil Kumar) and N.C. wrote and revised the article. All authors proofread and approved the final version of the manuscript.

Data availability statement

The data that support the findings of this study are openly available in ProteomeXchange consortium at https://www.proteomexchange.org/, reference number PXD022269.

References

Aguiar, A.S., Costa, L.B., Borges, I.D., Aguirre, G., Tejerina-Garro, F.L., Dutra e Silva, S. and Napolitano, H.B. (2023) The effect of water molecules on paraquat salts: from physicochemical properties to environmental impact in the Brazilian Cerrado. *Front. Chem.* **11**, 1267634.

Albus, C.A., Salinas, A., Czarnecki, O., Kahlau, S., Rothbart, M., Thiele, W., Lein, W. *et al.* (2012) LCAA, a novel factor required for magnesium protoporphyrin monomethylester cyclase accumulation and feedback control of aminolevulinic acid biosynthesis in tobacco. *Plant Physiol.* **160**, 1923–1939.

Atkin, O.K. and Macherel, D. (2008) The crucial role of plant mitochondria in orchestrating drought tolerance. *Ann. Bot.* **103**, 581–597.

Bardel, J., Louwagie, M., Jaquinod, M., Jourdain, A., Luche, S., Rabilloud, T., Macherel, D. *et al.* (2002) A survey of the plant mitochondrial proteome in relation to development. *Proteomics*, **2**, 880–898.

Baudisch, B. and Klosgen, R.B. (2012) Dual targeting of a processing peptidase into both endosymbiotic organelles mediated by a transport signal of unusual architecture. *Mol. Plant*, **5**, 494–503.

Bhushan, D., Pandey, A., Choudhary, M.K., Datta, A., Chakraborty, S. and Chakraborty, N. (2007) Comparative proteomic analysis of differentially expressed proteins in chickpea extracellular matrix during dehydration stress. *Mol. Cell. Proteomics*, **6**, 1868–1884.

Blum, A. (2009) Effective use of water (EUW) and not water-use efficiency (WUE) is the target of crop yield improvement under drought stress. *Field Crop Res.* **112**, 119–123.

Bournonville, C.F.G. and Diaz-Ricci, J.C. (2011) Quantitative determination of superoxide in plant leaves using a modified NBT staining method. *Phytochem. Anal.* **22**, 268–271.

Carrie, C., Venne, A.S., Zahedi, R.P. and Soll, J. (2015) Identification of cleavage sites and substrate proteins for two mitochondrial intermediate peptidases in *Arabidopsis thaliana*. *J. Exp. Bot.* **66**, 2691–2708.

Castillo, F.J., Penel, C. and Greppin, H. (1984) Peroxidase release induced by ozone in Sedum album leaves: involvement of Ca2+. *Plant Physiol.* **74**, 846–851.

Chen, G.E. and Hunter, C.N. (2020) Protochlorophyllide synthesis by recombinant cyclases from eukaryotic oxygenic phototrophs and the dependence on Ycf54. *Biochem. J.* **477**, 2313–2325.

Chen, X., Wang, Y., Li, J., Jiang, A., Cheng, Y. and Zhang, W. (2009) Mitochondrial proteome during salt stress-induced programmed cell death in rice. *Plant Physiol. Biochem.* **47**, 407–415.

Choudhary, M.K., Basu, D., Datta, A., Chakraborty, N. and Chakraborty, S. (2009) Dehydration-responsive nuclear proteome of rice (*Oryza sativa* L.) illustrates protein network, novel regulators of cellular adaptation, and evolutionary perspective. *Mol. Cell. Proteomics*, **8**, 1579–1598.

Cocheme, H.M. and Murphy, M.P. (2008) Complex I is the major site of mitochondrial superoxide production by paraquat. *J. Biol. Chem.* **283**, 1786–1798.

Cox, A.G., Winterbourn, C.C. and Hampton, M.B. (2010) Mitochondrial peroxiredoxin involvement in antioxidant defence and redox signalling. *Biochem. J.* **425**, 313–325.

Cui, F., Brosche, M., Shapiguzov, A., He, X.Q., Vainonen, J.P., Leppala, J., Trotta, A. *et al.* (2019) Interaction of methyl viologen-induced chloroplast and mitochondrial signalling in Arabidopsis. *Free Radic. Biol. Med.* **134**, 555–566.

Dietz, K.J. (2011) Peroxiredoxins in plants and cyanobacteria. *Antioxid. Redox Signal.* **15**, 1129–1159.

Dietz, K.J. and Pfannschmidt, T. (2011) Novel regulators in photosynthetic redox control of plant metabolism and gene expression. *Plant Physiol.* **155**, 1477–1485.

Dubinin, J., Braun, H.P., Schmitz, U. and Colditz, F. (2011) The mitochondrial proteome of the model legume *Medicago truncatula*. *Biochim. Biophys. Acta*, **1814**, 1658–1668.

Dunn, J.D., Alvarez, L.A., Zhang, X. and Soldati, T. (2015) Reactive oxygen species and mitochondria: a nexus of cellular homeostasis. *Redox Biol.* **6**, 472–485.

Gayen, D., Gayali, S., Barua, P., Lande, N.V., Varshney, S., Sengupta, S., Chakraborty, S. *et al.* (2019) Dehydration-induced proteomic landscape of

mitochondria in chickpea reveals large-scale coordination of key biological processes. *J. Proteome*, **192**, 267–279.

Gho, Y.S., Park, S.A., Kim, S.R., Chandran, A.K.N., An, G. and Jung, K.H. (2017) Comparative expression analysis of rice and Arabidopsis peroxiredoxin genes suggests conserved or diversified roles between the two species and leads to the identification of tandemly duplicated rice peroxiredoxin genes differentially expressed in seeds. *Rice*, **10**, 1–14.

He, F., Chen, S., Ning, Y. and Wang, G.L. (2016) Rice (Oryza sativa) protoplast isolation and its application for transient expression analysis. *Current protocols in Plant Biol.* **1**, 373–383.

He, J., Duan, Y., Hua, D., Fan, G., Wang, L., Liu, Y., Chen, Z. *et al*. (2012) DEXH box RNA helicase–mediated mitochondrial reactive oxygen species production in Arabidopsis mediates crosstalk between abscisic acid and auxin signaling. *Plant Cell*, **24**, 1815–1833.

Herbst, J., Girke, A., Hajirezaei, M.R., Hanke, G. and Grimm, B. (2018) Potential roles of YCF54 and ferredoxin-NADPH reductase for magnesium protoporphyrin monomethylester cyclase. *Plant J.* **94**, 485–496.

Hollingshead, S., Kopecna, J., Armstrong, D.R., Bucinska, L., Jackson, P.J., Chen, G.E., Dickman, M.J. *et al*. (2016) Synthesis of chlorophyll-binding proteins in a fully segregated Δycf54 strain of the cyanobacterium Synechocystis PCC 6803. *Front. Plant Sci.* **7**, 292.

Huang, S., Taylor, N.L., Narsai, R., Eubel, H., Whelan, J. and Millar, A.H. (2009) Experimental analysis of the rice mitochondrial proteome, its biogenesis, and heterogeneity. *Plant Physiol.* **149**, 719–734.

Huang, S., Van Aken, O., Schwarzlander, M., Belt, K. and Millar, A.H. (2016) The roles of mitochondrial reactive oxygen species in cellular signaling and stress response in plants. *Plant Physiol.* **171**, 1551–1559.

Jacoby, R.P., Li, L., Huang, S., Lee, C.P., Millar, A.H. and Taylor, N.L. (2012) Mitochondrial composition, function and stress response in plants. *J. Integr. Plant Biol.* **54**, 887–906.

Jacoby, R.P., Millar, A.H. and Taylor, N.L. (2010) Wheat mitochondrial proteomes provide new links between antioxidant defense and plant salinity tolerance. *J. Proteome Res.* **9**, 6595–6604.

Jain, M., Nijhawan, A., Arora, R., Agarwal, P., Ray, S., Sharma, P., Kapoor, S. *et al*. (2007) F-box proteins in rice. Genome-wide analysis, classification, temporal and spatial gene expression during panicle and seed development, and regulation by light and abiotic stress. *Plant Physiol.* **143**, 1467–1483.

Jing, L.W., Chen, S.H., Guo, X.L., Zhang, H. and Zhao, Y.X. (2006) Overexpression of a chloroplast-located peroxiredoxin Q gene, SsPrxQ, increases the salt and low-temperature tolerance of Arabidopsis. *J. Integr. Plant Biol.* **48**, 1244–1249.

Karmakar, S., Molla, K.A., Chanda, P.K., Sarkar, S.N., Datta, S.K. and Datta, K. (2016) Green tissue-specific co-expression of chitinase and oxalate oxidase 4 genes in rice for enhanced resistance against sheath blight. *Planta*, **243**, 115–130.

Kaur, N., Sharma, I., Kirat, K. and Pati, P.K. (2016) Detection of reactive oxygen species in *Oryza sativa* L. (rice). *Bio Protoc.* **6**, 2061.

Komatsu, S., Yamamoto, A., Nakamura, T., Nouri, M.Z., Nanjo, Y., Nishizawa, K. and Furukawa, K. (2011) Comprehensive analysis of mitochondria in roots and hypocotyls of soybean under flooding stress using proteomics and metabolomics techniques. *J. Proteome Res.* **10**, 3993–4004.

Lahtvee, P.J., Kumar, R., Hallström, B.M. and Nielsen, J. (2016) Adaptation to different types of stress converge on mitochondrial metabolism. *Mol. Biol. Cell*, **27**, 2505–2514.

Lamkemeyer, P., Laxa, M., Collin, V., Li, W., Finkemeier, I., Schottler, M.A., Holtkamp, V. *et al*. (2006) Peroxiredoxin Q of *Arabidopsis thaliana* is attached to the thylakoids and functions in context of photosynthesis. *Plant J.* **45**, 968–981.

Lasanthi-Kudahettige, R., Magneschi, L., Loreti, E., Gonzali, S., Licausi, F., Novi, G., Beretta, O. *et al*. (2007) Transcript profiling of the anoxic rice coleoptile. *Plant Physiol.* **144**, 218–231.

Lee, C.P., Eubel, H., O'Toole, N. and Millar, A.H. (2008) Heterogeneity of the mitochondrial proteome for photosynthetic and non-photosynthetic Arabidopsis metabolism. *Mol. Cell. Proteomics*, **7**, 1297–1316.

Lee, C.P., Eubel, H., O'Toole, N. and Millar, A.H. (2011) Combining proteomics of root and shoot mitochondria and transcript analysis to define constitutive and variable components in plant mitochondria. *Phytochemistry*, **72**, 1092–1108.

Li, C.R., Liang, D.D., Li, J., Duan, Y.B., Li, H., Yang, Y.C., Qin, R.Y. *et al*. (2013) Unravelling mitochondrial retrograde regulation in the abiotic stress induction of rice ALTERNATIVE OXIDASE 1 genes. *Plant Cell Environ.* **36**, 775–788.

Li, Y., Gao, Y., Xu, X., Shen, Q. and Guo, S. (2009) Light-saturated photosynthetic rate in high-nitrogen rice (*Oryza sativa* L.) leaves is related to chloroplastic CO_2 concentration. *J. Exp. Bot.* **60**, 2351–2360.

Li, Y., Liang, G., Nai, G., Lu, S., Ma, W., Ma, Z., Mao, J. *et al*. (2023) VaSUS2 confers cold tolerance in transgenic tomato and Arabidopsis by regulation of sucrose metabolism and ROS homeostasis. *Plant Cell Rep.* **42**, 505–520.

Ma, X., Zhang, Q., Zhu, Q., Liu, W., Chen, Y., Qiu, R., Wang, B. *et al*. (2015) A robust CRISPR/Cas9 system for convenient, high-efficiency multiplex genome editing in monocot and dicot plants. *Mol. Plant*, **8**, 1274–1284.

Michaud, M., Marechal-Drouard, L. and Duchene, A.M. (2010) RNA trafficking in plant cells: targeting of cytosolic mRNAs to the mitochondrial surface. *Plant Mol. Biol.* **73**, 697–704.

Millar, A.H., Trend, A.E. and Heazlewood, J.L. (2004) Changes in the mitochondrial proteome during the anoxia to air transition in rice focus around cytochrome-containing respiratory complexes. *J. Biol. Chem.* **279**, 39471–39478.

Moller, I.M., Liden, A.C., Ericson, I. and Gardestrom, P. (1987) Isolation of submitochondrial particles with different polarities. *Meth. Enzymol.* **148**, 442–453.

Mustafa, G. and Komatsu, S. (2016) Insights into the response of soybean mitochondrial proteins to various sizes of aluminium oxide nanoparticles under flooding stress. *J. Proteome Res.* **15**, 4464–4475.

Rouhier, N., Gelhaye, E., Gualberto, J.M., Jordy, M.N., De Fay, E., Hirasawa, M., Duplessis, S. *et al*. (2004) Poplar peroxiredoxin Q. A thioredoxin-linked chloroplast antioxidant functional in pathogen defense. *Plant Physiol.* **134**, 1027–1038.

Rurek, M., Czołpinska, M., Pawłowski, T., Krzesinski, W. and Spizewski, T. (2018) Cold and heat stress diversely alter both cauliflower respiration and distinct mitochondrial proteins including OXPHOS components and matrix enzymes. *Int. J. Mol. Sci.* **19**, 877.

Salvato, F., Havelund, J.F., Rao RSP, C.M., Rogowska-Wrzesinska, A., Jensen, O.N., Gang, D.R., Thelen, J.J. *et al*. (2014) The potato tuber mitochondrial proteome. *Plant Physiol.* **164**, 637–653.

Sandalio, L.M. and Romero-Puertas, M.C. (2015) Peroxisomes sense and respond to environmental cues by regulating ROS and RNS signalling networks. *Ann. Bot.* **116**, 475–485.

Schurmann, P. and Jacquot, J.P. (2000) Plant thioredoxin systems revisited. *Annu. Rev. Plant Biol.* **51**, 371–400.

Sevilla, F., Camejo, D., Ortiz-Espin, A., Calderon, A., Lazaro, J.J. and Jimenez, A. (2015) The thioredoxin/peroxiredoxin/sulfiredoxin system: current overview on its redox function in plants and regulation by reactive oxygen and nitrogen species. *J. Exp. Bot.* **66**, 2945–2955.

Shapiguzov, A., Vainonen, J.P., Hunter, K., Tossavainen, H., Tiwari, A., Jarvi, S., Hellman, M. *et al*. (2019) Arabidopsis RCD1 coordinates chloroplast and mitochondrial functions through interaction with ANAC transcription factors. *eLife*, **8**, 43284.

Smakowska, E., Blaszczyk, R.S., Czarna, M., Kolodziejczak, M., Owczarek, M.K., Parys, K., Funk, C. *et al*. (2016) Lack of FTSH4 protease affects protein carbonylation, mitochondrial morphology and phospholipid content in mitochondria of Arabidopsis: new insights into a complex interplay. *Plant Physiol.* **171**, 2516–2535.

Sweetlove, L.J., Heazlewood, J.L., Herald, V., Holtzapffel, R., Day, D.A., Leaver, C.J. and Millar, A.H. (2002) The impact of oxidative stress on Arabidopsis mitochondria. *Plant J.* **32**, 891–904.

Tan, Y.F., Millar, A.H. and Taylor, N.L. (2012) Components of mitochondrial oxidative phosphorylation vary in abundance following exposure to cold and chemical stresses. *J. Proteome Res.* **11**, 3860–3879.

Taylor, N.L., Heazlewood, J.L., Day, D.A. and Millar, A.H. (2005) Differential impact of environmental stresses on the pea mitochondrial proteome. *Mol. Cell Proteomics* **4**, 1122–1133.

Timm, S., Wittmib, M., Gamlien, S., Ewald, R., Florian, A., Frank, M., Wirtz, M. *et al*. (2015) Mitochondrial dihydrolipoyl dehydrogenase activity shapes photosynthesis and photorespiration of *Arabidopsis thaliana*. *Plant Cell*, **27**, 1968–1984.

Tran, K. and Green, E.M. (2019) Assessing yeast cell survival following hydrogen peroxide exposure. *Bio Protoc.* **9**, e3149.

Wang, S., Zhang, G., Zhang, Y., Song, Q., Chen, Z., Wang, J., Guo, J. *et al*. (2015) Comparative studies of mitochondrial proteomics reveal an intimate protein network of male sterility in wheat (*Triticum aestivum* L.). *J. Exp. Bot.* **66**, 6191–6203.

Wang, W.Q., Wang, Y., Zhang, Q., Møller, I.M. and Song, S.Q. (2018) Changes in the mitochondrial proteome of developing maize seed embryos. *Physiol. Plant.* **163**, 552–572.

Xie, K., Minkenberg, B. and Yang, Y. (2015) Boosting CRISPR/Cas9 multiplex editing capability with the endogenous tRNA-processing system. *Proc. Natl. Acad. Sci. USA*, **112**, 3570–3575.

Xu, J., Du, N., Dong, T., Zhang, H., Xue, T., Zhao, F., Zhao, F. *et al*. (2023) A novel *Pinellia ternata* catalase gene PtCAT2 regulates drought tolerance in Arabidopsis by modulating ROS balance. *Front. Plant Sci.* **14**, 1206798.

Zhou, Y., Liu, C., Tang, D., Yan, L., Wang, D., Yang, Y., Zhao, X.Y. *et al*. (2018) The receptor-like cytoplasmic kinase STRK1 phosphorylates and activates CatC, thereby regulating H_2O_2 homeostasis and improving salt tolerance in rice. *Plant Cell*, **30**, 1100–1118.

Supporting information

Additional supporting information may be found online in the Supporting Information section at the end of the article.

Figure S1 Diagrammatic representation of experimental design depicting iTRAQ-based quantitative proteomic analysis.
Figure S2 Mitochondrial proteome landscape of rice.
Figure S3 Categorization of DRPs identified in mitochondrial proteome.
Figure S4 Species-wide mitochondrial proteome diversity.
Figure S5 Dehydration-induced transcriptional regulation of randomly selected DRPs and spatial expression of OsDUF2488.
Figure S6 Genomic organization, phylogenetic profiling and stress-induced expression of OsDUF2488.
Figure S7 Optimization of aureobasidin A concentration in Y2H screening and proteins identified.
Figure S8 Proteome-wide interactome network of mitochondrial DRPs and expression of OsDUF2488 and OsPrx1.
Figure S9 Interaction of OsDUF2488 and OsPrx1.1.
Figure S10 Multiple sequence alignment comparison of OsDUF2488 cDNA in cv. IR64 and Rasi.
Figure S11 Agronomic trait analysis in OsDUF2488-OE plants.
Figure S12 Validation of CRISPR/Cas9-mediated targeting mutagenesis OsDUF2488 in rice protoplasts.
Figure S13 Gel image showing PCR amplification of T_0 transgenic mutant lines targeting the *Cas9* gene.
Table S1 List of mitochondrial proteins identified by LC–MS/MS with more than two peptides (FDR 1%) and unused score ≥1.3.
Table S2 List of DRPs exhibiting upregulation by more than 1.5-fold and decreased abundance by less than 0.67-fold when compared to those in well-watered control plants in at least 2 replicates.
Table S3 Cross-species comparison of mitochondrial proteins in plants.
Table S4 Comparison of dehydration-responsive mitochondrial proteins in rice with previously reported stress-responsive mitochondrial proteins.
Table S5 Localization prediction of DUF2488 domain-containing proteins reported in Pfam database.
Table S6 List of proteins co-immunoprecipitated with OsDUF2488.
Table S7 Primer sequences used in this study.
Table S8 Off-target of mutant lines.